TECHNICAL MEMORANDUM

X-739

TRANSONIC FLUTTER INVESTIGATION OF MODELS OF A PROPOSED VARIABLE-SWEEP WING

By Charles L. Ruhlin and John R. Gurley, Jr.

Langley Research Center
Langley Station, Hampton, Va.

NATIONAL AERONAUTICS AND SPACE ADMINISTRATION
WASHINGTON December 1962

DEC[redacted]SIFIED

NATIONAL AERONAUTICS AND SPACE ADMINISTRATION

TECHNICAL MEMORANDUM X-739

TRANSONIC FLUTTER INVESTIGATION OF MODELS OF A PROPOSED VARIABLE-SWEEP WING*

By Charles L. Ruhlin and John R. Gurley, Jr.

SUMMARY

A transonic flutter investigation has been made of models which were dynamically and elastically scaled from a proposed variable-sweep wing design which had an aspect ratio of 7 (at minimum sweep), a taper ratio of 0.2, a fixed root section having a 65° sweepback angle, and a movable outboard panel. The elastic restraint at the pivot was simulated on the models. Models of the proposed wing and models of aspect ratio 5, formed by cutting off the tips from the proposed-wing models, were investigated with the outboard wing panel at leading-edge sweepback angles of 20°, 45°, 65°, and 80°. The flutter tests were conducted in the Langley transonic blowdown tunnel at Mach numbers from about 0.7 to 1.25.

Flutter boundaries were obtained for all configurations except the 80° swept, aspect-ratio-5 wing which was flutter-free within the test limits available in the tunnel. In general, the transonic flutter boundaries obtained were typical of those for wings of moderate aspect ratio. At subsonic Mach numbers, increasing the sweep angle of a wing increased the dynamic pressure required for flutter. The results suggest that stiffness requirements established by flutter considerations may be minimized by flight programing of the sweepback angle for wings similar to the present two designs.

INTRODUCTION

A number of variable-geometry wing configurations have been considered for supersonic transports (refs. 1 and 2) and STOL aircraft. One configuration which has received considerable study is the variable-sweep wing consisting of a fixed root section and an outboard, movable panel that can be rotated through a wide range of sweepback angles during flight. Structural deformation tests and vibration studies of a one-half-size, simplified model of a variable-sweep wing have been reported

---

[redacted]

[redacted]

in reference 3. Experimental flutter trends of simplified models of a variable-sweep wing configuration have been obtained at transonic and supersonic speeds in reference 4. However, no pivot flexibility was simulated in the models of reference 4, instead three different planforms were used to represent the variable-sweep wing at sweepback angles of 25°, 60°, and 75°, respectively.

In the present investigation the transonic flutter characteristics were determined for models which were dynamically and elastically scaled from a proposed variable-sweep wing design. In addition, the models simulated the elastic restraint at the pivot joint. The wing design had an aspect ratio of about 7 in the minimum-sweep condition, a taper ratio of about 0.2, a modified NACA 64-209 airfoil section measured perpendicular to the wing trailing edge, and a movable outboard panel that could be rotated to sweepback angles from 20° to 80° measured at the leading edge. The fixed root section had a leading-edge sweepback angle of 65°, a pivot at the outer extremity, and a track located inboard. Since planforms of lower aspect ratios had also been considered for the proposed variable-sweep wing, the flutter characteristics were determined for an aspect-ratio-5 planform which was formed by cutting off a tip segment of the aspect-ratio-7 wing.

The flutter tests were conducted in the Langley transonic blowdown tunnel and covered a Mach number range from about 0.70 to 1.25. Both planforms were investigated with the wing sweepback angle set at 20°, 45°, 65°, and 80°.

SYMBOLS

a speed of sound, ft/sec

b one-half mean aerodynamic chord, measured normal to elastic axis, ft

c wing chord measured normal to elastic axis, ft

EI bending stiffness, lb-in.^{2}

f frequency at flutter or during low damping period, cps

$f_{h,i}$ measured resonant vibration frequency of ith bending mode $(i = 1, 2, 3)$, cps

f_{yaw} measured resonant vibration frequ[redacted]cy i[redacted]

[redacted]

f_α, ω_α — measured resonant vibration frequency of first torsion mode, cps and radians/sec, respectively

$g_{h,1}$ — structural damping coefficient in first bending vibration mode

GJ — torsional stiffness, lb-in.^{2}

h — bending deflection, in.

h_o — reference bending deflection, in.

I_α — mass moment of inertia per unit length about elastic axis, $\frac{\text{slug-ft}^2}{\text{ft}}$

$$K_{h,L} = \frac{\text{Load at pivot}}{\text{Bending deflection at pivot due to load}}, \text{ lb/in.}$$

$$K_{h,M} = \frac{\text{Bending moment at pivot}}{\text{Bending deflection at pivot due to bending moment}}, \frac{\text{in-lb}}{\text{in.}}$$

$$K_\alpha = \frac{\text{Torque about elastic axis at pivot}}{\text{Twist at pivot due to torque}}, \frac{\text{in-lb}}{\text{radian}}$$

$$K_{\psi,L} = \frac{\text{Load at pivot}}{\text{Bending slope at pivot due to load}}, \text{ lb/radian}$$

$$K_{\psi,M} = \frac{\text{Bending moment at pivot}}{\text{Bending slope at pivot due to bending moment}}, \frac{\text{in-lb}}{\text{radian}}$$

m — mass of movable wing panel from pivot axis to tip, slugs

m_s — mass per unit length, slugs/ft

M — Mach number

q — dynamic pressure, lb/sq ft

q_{adj} — dynamic pressure adjusted to pertain to wing of selected reference stiffness level for each planform (see Presentation of Results), lb/sq ft

[redacted]

[redacted]

S_α static unbalance per unit length about the elastic axis, positive for center of gravity rearward of elastic axis, $\frac{\text{slug-ft}}{\text{ft}}$

T static temperature, $^{\circ}$R

v volume of frustrum of cone having base diameter equal to wing chord measured perpendicular to elastic axis at pivot axis, tip diameter equal to wing chord measured perpendicular to elastic axis at tip, and height equal to length of wing elastic axis from pivot axis to tip, cu ft

V stream velocity, ft/sec

x_α distance from elastic axis to wing-section center of gravity, measured perpendicular to elastic axis, positive rearward, ft

y spanwise wing station measured along elastic axis from root of butt spar, ft unless otherwise noted

y_{cg} distance along elastic axis from root of butt spar to wing-section center of gravity, ft

Λ sweepback angle of leading edge of movable outboard wing panel, deg

μ mass ratio, $m/\rho v$

ρ air density, slugs/cu ft

MODELS

Geometry

Sketches and photographs of the models are presented in figures 1 and 2. Two different wing planforms were investigated. One wing planform (fig. 1(a)), which simulated the proposed variable-sweep wing design, had an aspect ratio of 7 in the minimum-sweep condition, a taper ratio of about 0.2, a fixed root section which had a sweepback angle of 65°, and a movable outboard panel that could be rotated through a sweepback-angle range from 20° to 80°. (All sweepback angles used herein are measured at the wing leading edge.) The outboard panel had an NACA 64-209 airfoil section modified to a straight line aft of the 60-percent chord (measured perpendicul[redacted]r to wing trailing edge). The

[redacted]

second wing planform (fig. 1(b)), which was formed from the aspect-ratio-7 planform by cutting off a tip segment of the outboard panel, had an aspect ratio of 5 and a taper ratio of about 0.4. Both wing configurations were investigated at sweepback angles of 20°, 45°, 65°, and 80°. The wing pivot point was located at about 10 percent and 13 percent of the exposed semispan for the aspect-ratio-7 (AR-7) wing and for the aspect-ratio-5 (AR-5) wing, respectively, at a sweep angle of 20°.

Arrangement

Each outboard panel of the AR-7 wing was elastically and dynamically scaled from the movable outboard panel of the proposed variable-sweep wing design. The model outboard panel was attached to a beam (figs. 1(c) and 2(a)), designated as the butt spar, which provided the scaled elastic restraint at the pivot axis. When assembled, the butt spar was cantilevered from the fuselage-sting through a mounting block which could be mounted at the various sweepback angles on the fuselage mounting plate. The curved surfaces of the fuselage mounting plate and model mounting block were such that the centers of curvature were coincident with the wing theoretical pivot point. The geometry of the fixed root section was simulated by an aluminum sheet fairing (figs. 2(a) to 2(c)) which fitted around the butt spar and a small portion of the outboard wing panel. The inboard fairing was attached to the fuselage and, in fitting the fairing over the wing, a gap between the surfaces of the fairing and outboard wing panel was usually set at about one-eighth inch.

With this mounting arrangement, the frequencies and node lines of the models remained the same as the sweep angle was varied. Calculations made for the full-scale wing have indicated that the frequencies and node lines would change with sweep angle; however, these changes were relatively small and the present model arrangement was considered to adequately simulate the wing at the various sweep angles.

Each scaled semispan model was tested with a comparatively rigid dummy wing mounted on the opposite side of the fuselage. The dummy wing had the same geometry as the AR-7 wing and was used to approximate the aerodynamic loads which would be obtained with a full-span wing. Although the dummy panel was used in all of the tests, the aerodynamic load on the dummy panel was never considered to have any appreciable effect on the flutter of the elastic panel because of the nearly zero-lift condition of the model during testing and because of the end-plate effect of the fuselage.

[redacted]

Construction

X-ray photographs of typical outboard panels of the AR-7 wings are presented in figure 3. Each wing panel was of the spar-and-rib type of construction (fig. 3) with lead weights as ballast and with balsa wood to provide the airfoil contour. Narrow chordwise slots were cut in the balsa to obtain the correct stiffness distribution, and the wing panel and slots were covered by a thin, high-strength paper. Outboard panels and butt spars of four different stiffness levels (designated I to IV, from highest to lowest stiffness level) were constructed, and a number of models of each stiffness level were used in the tests. In general, the internal structure of the wing panels of stiffness levels II, III, and IV was the same (fig. 3(b)), differing only in the cross-section dimensions of the spars and ribs and the sizes of the lead ballast weights. The butt spars were short steel beams having cross sections similar to that shown in figure 1(c) over most of their spanwise lengths.

Properties

The mass of the AR-7 wings was the same for all stiffness levels and simulated the full-fuel condition of the proposed wing design. The measured mass properties of a typical model outboard panel and butt spar are presented in table I. Presented in figure 4 are the measured stiffness distributions of a typical model of each stiffness level and the various stiffnesses measured at the pivot axis of a typical butt spar of each stiffness level. The stiffness distributions were measured along or about the elastic axis which was assumed to be the center line of the wing spar (fig. 3) and was located at about 37 percent of the wing chord. It may be noted in table I that the values of S_α and x_α are very small indicating that the centers of gravity of the wing sections are near the elastic axis.

The measured resonant vibration frequencies of the models are presented in table II, and typical node lines associated with these frequencies are presented in figure 5. The node lines for the various wings of each planform were found to be generally the same. Included in table II are the measured structural damping coefficients in the first bending mode. The measured mode shapes of the first four natural vibration modes of a typical AR-7 wing panel of each stiffness level are shown in figure 6.

Comparison of the vibration frequencies for the two planforms (table II) indicates that cutting off the relatively flexible tip from an AR-7 wing to form an AR-5 wing caused a large increase in the bending frequencies but only a small increase in the torsion frequency; and, as a result, the frequency spectrums of the two wings were considerably

[redacted]

different. The nodal patterns (fig. 5) indicate that the vibration modes for these wings were essentially uncoupled modes. The mode shapes of the AR-7 wing (fig. 6) were nearly the same for the various stiffness levels, as would be expected for wings having the same mass distributions and the same stiffness distributions.

TEST APPARATUS AND TECHNIQUE

The flutter tests were conducted in the Langley transonic blowdown tunnel at Mach numbers from about 0.7 to 1.25. The tunnel has a slotted, octagonal test section which measures 26 inches between flats. The tunnel is particularly useful for flutter investigations because Mach number and air density may be varied independently.

For each run the model wing and dummy wing panel were mounted in a cylindrical fuselage-sting which was 3.40 inches in diameter. The fuselage-sting extended upstream into the subsonic flow region of the tunnel in order to prevent the formation of bow shock waves. The sting was installed at two different locations in the tunnel. In one location which is shown in figure 7, the sting was mounted to the tunnel wall so that the sting lay along the center line of the tunnel. In the other sting location, which was used for most of the runs, the sting was mounted to the tunnel wall so that the sting center line was about 5 inches away from but parallel to the tunnel center line. The off-center sting location was necessary to provide an acceptable clearance between the tunnel wall and the tip of the 20° swept, AR-7 wing. At either location, the sting with the model installed had a fundamental bending frequency of about 18 cps.

The model wing and dummy wing panel were installed in the fuselage-sting at an angle of attack for approximately zero lift. The dummy wing panel was installed at the same sweepback angle as that for the model wing with two exceptions: for the tests of the AR-7 wing at 20° and 45° sweep, the dummy panel was mounted at a sweep angle of 65° which was the minimum sweep angle that the dummy panel could be installed with the off-center sting in the tunnel.

The tunnel operating characteristics for three typical runs are presented in figure 8, where the variations of dynamic pressure with Mach number are shown for fixed-orifice and varying-orifice operating procedures. The technique employed in most runs was, with a fixed orifice, to increase the stagnation pressure gradually until either flutter occurred or the desired dynamic-pressure level was reached. In some runs a predetermined dynamic-pressure level was reached and then the tunnel orifice was varied so that a variation of dynamic pressure over a Mach number range was obtained.

[redacted]

[redacted]

During each run, the model was visually observed through a viewing screen in the tunnel control room. When flutter was observed, the tunnel was instantly shut down to prevent or reduce model damage. The output of the strain gages on the model, the test-section stagnation and static pressures, and the stagnation temperature were continuously recorded during a run by means of a recording oscillograph. The records of the strain-gage outputs were used to indicate the occurrence of flutter and the flutter frequencies. Models used in more than one run were checked for structural damage by visual inspection and by comparing natural frequencies measured in the tunnel before and after each run. High-speed motion pictures (approximately 1,000 frames per second) were taken of the model to provide a visual record of the model behavior during a run.

PRESENTATION OF RESULTS

The results of the flutter tests are presented in table III. The table is self-explanatory with the following exceptions. A number of data points were sometimes obtained during a single run, and each data point is listed (column 2, table III) in the order from the beginning of the run in which it occurred. A low damping region (D) is a region of doubtful flutter characterized by intermittent sinusoidal oscillations of the model; a burst of low damping (BD) indicates a region where low damping occurred but where there was no significant change in the tunnel conditions between the start and stop of the low damping period. A number of no-flutter points (NF) are included in the results as an aid in defining the flutter boundaries and as an indication of the no-flutter regions covered in the investigation.

In order to obtain flutter at the various sweepback angles, wings of different stiffness levels were tested. The dynamic pressures obtained for the tested wings were adjusted to apply to a wing of one stiffness level for each planform, and the adjusted dynamic pressures q_{adj} are included in table III. The adjustment to the dynamic pressures was based on a procedure which past experience has proved applicable to a wide variety of models. The procedure is derived from the relationship that the flutter-speed index $\frac{V}{b\omega_\alpha\sqrt{\mu}}$ is a constant for wings which have the same planform, the same stiffness distribution, and the same mass distribution, regardless of the level of mass or stiffness. Thus

$$\left(\frac{V}{b\omega_\alpha\sqrt{\mu}}\right)_i = \left(\frac{V}{b\omega_\alpha\sqrt{\mu}}\right)_j$$

[redacted]AL

where i refers to stiffness level i, and j refers to stiffness level j. This relationship is valid provided that at any given Mach number the mass ratio μ at flutter or at a test condition is the same for the various wings. In the present tests, the values of μ were not the same for the tested wings; however, past experience has indicated that in the range of μ for most of the present tests, the effects of the present differences in the mass ratios are small and may usually be neglected. The equation may be reduced to

$$q_{adj} = q_j \frac{{f_{\alpha,i}}^2}{{f_{\alpha,j}}^2}$$

where q_{adj} is the dynamic pressure adjusted to pertain to a model of the ith or reference stiffness level, and q_j and $f_{\alpha,j}$ are the experimental dynamic pressure and torsional frequency, respectively, for a wing of the jth stiffness level. A stiffness level of I was arbitrarily selected as the reference stiffness level for the AR-7 wings, and a stiffness level of IV as the reference stiffness level for the AR-5 wings. The average value of the torsional frequency measured for the wings of each reference stiffness level (table II) was used for the value of $f_{\alpha,i}$; thus, for the AR-7 wing, $f_{\alpha,i} = 514$ cps, and for the AR-5 wing, $f_{\alpha,i} = 289$ cps.

The variations of the ratio of flutter frequency to torsion frequency with Mach number for the AR-7 and AR-5 wings are presented in figure 9. The ranges of the ratios of bending frequency to torsion frequency which were measured for the models at zero airspeed are indicated on the ordinate scales of figure 9.

The results are presented in figure 10 as the variation with Mach number of the flutter-speed index $\frac{V}{b\omega_\alpha\sqrt{\mu}}$ and in figures 11 and 12 as the variation with Mach number of the adjusted dynamic pressures. In figure 13, the flutter boundaries of the AR-7 wing are shown along with three typical simulated altitude lines. The lines connecting some of the data points of figure 10 show the regions covered during runs in which the orifice plate was varied, and the arrows superimposed on these lines indicate the order in which these points were obtained. The data points from which the flutter boundaries of figures 11 and 12 were drawn are not shown in these figures.

[redacted]

DISCUSSION OF RESULTS

Flutter Modes and Frequencies

Aspect-ratio-7 wing.- From studies of the high-speed motion pictures taken during the tests, the flutter mode of the AR-7 wing appeared to gradually change with increase in sweepback angle from a mode involving a combination of the first and second bending modes and first torsion mode to a mode involving principally the second bending mode. At sweepback angles of 65° and 80°, the flutter appeared to be a type of tip flutter in which the amplitude of the motion at the wing tip was very large relative to that portion of the wing inboard of the second bending node (fig. 5), and there appeared to be only a slight amount of twist about the elastic axis. The flutter frequencies for the four sweepback angles (fig. 9(a)) were between the frequencies of the second and third bending natural-vibration modes (for zero airspeed), and less than the torsion frequency. Increasing the sweepback angle increased the flutter-frequency ratio with the exception that the flutter-frequency ratio for the 80° swept wing was less than that for the 65° swept wing throughout most of the Mach number range.

Aspect-ratio-5 wing.- The AR-5 wing appeared to flutter in a classical bending-torsion flutter mode at sweepback angles from 20° to 65°, and no flutter was obtained at the 80° sweep angle. The change in flutter mode from that for the AR-7 wing was not unexpected because the frequency spectrums for the two planforms were quite different (table II). The flutter frequencies of the AR-5 wing were between the frequencies of the first and second bending modes in contrast to the flutter frequencies of the AR-7 wing which were between the frequencies of the second and third bending modes. A similar trend of increasing flutter frequency with increasing sweep angle was obtained with the AR-5 wing as was obtained with the AR-7 wing.

Flutter Boundaries

The results of the present investigation are presented in figure 10 as the variation with Mach number of the flutter-speed index $\frac{V}{b\omega_{\alpha}\sqrt{\mu}}$ and are compared in figures 11 and 12 in terms of the adjusted dynamic pressure, which is proportional to the flutter-speed index. Because of the scatter in the experimental data, some judgment was required in drawing the flutter boundaries of figures 10, 11, and 12, and it is realized that different boundaries could reasonably be drawn from the present data.

[redacted]

As mentioned previously, there was approximately a 1/8-inch gap between the fixed inboard fairing and the surface of the movable wing panel. In order to determine the effect of this gap on the wing flutter, several tests were made at the higher Mach numbers of an AR-7 wing at 80° sweep with the sheet-metal fairing replaced by a light balsa fairing attached directly to the wing panel. The balsa fairing was contoured so that there was no appreciable gap between the fairing and wing panel. The effect of the fairing change was somewhat obscured by the scatter in the test data, but did not appear to be significant.

Aspect-ratio-7 wing.- The flutter boundaries shown in figure 11 may be considered as the dynamic pressures at which an AR-7 wing of stiffness level I would flutter with the wing set at sweepback angles of 20°, 45°, 65°, and 80°. These flutter boundaries exhibit characteristics typical of a number of configurations at transonic speeds; for example, the flutter boundaries for the wings investigated in reference 4. At $M = 0.8$, the dynamic pressure at which flutter occurred for the 45°, 65°, and 80° swept wing was about 1.3, 1.9, and 2.0 times greater, respectively, than that for the 20° swept wing. The Mach number at which the transonic dip occurred increased with sweep angle up to 65°. For the 80° swept wing, the transonic dip occurred at a Mach number lower than that for the 65° swept wing.

Aspect-ratio-5 wing.- The flutter boundaries shown in figure 12 may be considered as the variation with Mach number of the dynamic pressures at which an AR-5 wing of stiffness level IV would flutter at 20°, 45°, and 65° sweepback angles. Included in this figure are the no-flutter points for the 80° swept wing. In general, the flutter boundaries are typical of those for wings at transonic speeds except that the 45° and 65° swept wings appear to have only a slight, if any, transonic dip. Although the flutter boundary for the 45° swept wing is not well defined in the Mach number region where a dip might be expected (fig. 10(b)), the low damping regions extending from Mach numbers of about 1.05 to 1.15 strongly suggest a flutter boundary near these dynamic pressures. At a Mach number of 0.8, the 45° and 65° swept wings required a dynamic pressure for flutter 1.2 and 2.6 times greater, respectively, than did the 20° swept wing, and the 80° swept wing was flutter-free to a dynamic pressure at least 2.0 times greater than the flutter dynamic pressure for the 20° swept wing.

A comparison of the flutter boundaries for the AR-7 and AR-5 planforms (figs. 11 and 12) shows that the percentage increase in the dynamic pressure for flutter obtained by increasing the sweep angle from 20° to 45° at subsonic speeds was about the same for the two planforms. The 20° swept wings exhibited generally the same flutter trends with the transonic dip for the AR-5 wing occurring at a higher Mach number and extending over a broader Mach number range. Comparison of the 45° and 65° swept wings loses some significance because the flutter boundaries

[redacted]

of the AR-5 wing are not very well defined at the transonic Mach numbers. However, it is seen that the transonic dip for the AR-5 wings is probably less severe than that for the AR-7 wing, and for the 45° swept wing the sharp increase in flutter dynamic pressure following the transonic region occurs at a considerably higher Mach number for the AR-5 wing than for the AR-7 wing. These differences in the flutter boundaries of the two planforms are attributed not only to the aerodynamic effects of changing the aspect ratio, but also to the difference in the vibration modes and frequency spectrums which have a large effect on the flutter mode.

Sweep Scheduling to Avoid Flutter

The present results suggest the possibility of avoiding flutter regions by proper flight programing of the wing sweepback angles. In order to demonstrate possible sweep-angle scheduling, the flutter boundaries of the AR-7 wing are shown in figure 13 along with three simulated, constant-altitude lines. Altitude A represents a low altitude, B represents an intermediate altitude, and C a higher altitude. These altitude lines were assumed to have included a flutter safety margin in the dynamic pressure of 32 percent, that is, the simulated dynamic pressure at a given altitude and Mach number has been increased by 32 percent. Let it also be assumed that only sweep angles of 20°, 45°, 65°, and 80° would be used in the sweep scheduling. Thus, for flight with a flutter safety margin at a given altitude, the altitude line must be below the flutter boundary (fig. 13) for the sweep angle at which the airplane wing is set. For example, at altitude C, the airplane could fly at any sweep angle over the Mach number range shown. For flight at altitude B, a sweep angle of 45° or greater would be required at Mach numbers from about 0.88 to 0.95. For flight at altitude A several sweep programs could be used. One sweep program, for which the minimum sweep angle would be obtained over the greatest Mach number range, would be to increase the sweep angle from 20° to 45° at $M = 0.74$, increase the sweep from 45° to 65° at $M = 0.84$, and go to the maximum sweep (80°) at $M = 0.96$. It may be seen that at any of the three altitudes, a sweep angle of 80° could be used throughout the Mach number range for which the flutter boundaries were determined. Thus by flight programing of the wing sweepback angle an adequate flutter safety margin may be obtained without increasing the wing stiffness level.

CONCLUSIONS

A transonic flutter investigation has been conducted of models of aspect ratio 7 (AR-7) which were dynamically and elastically scaled from a proposed variable-sweep wing design and of models of aspect ratio 5 (AR-5) which were formed by cutting off the tips from the models of the proposed wing. The results of flutter tests with the movable outboard

[redacted]

panels at leading-edge sweepback angles of 20°, 45°, 65°, and 80° have indicated the following:

1. In general, the transonic flutter boundaries obtained were typical of those for wings of moderate aspect ratios.

2. At a Mach number of 0.8, the AR-7 wing at sweepback angles of 45°, 65°, and 80° required a dynamic pressure for flutter 1.3, 1.9, and 2.0 times greater, respectively, than that for the 20° swept wing.

3. At a Mach number of 0.8, the AR-5 wing at sweepback angles of 45° and 65° required a dynamic pressure for flutter 1.2 and 2.6 times greater, respectively, than that required for 20° sweep, and the 80° swept configuration was flutter-free to a dynamic pressure at least 2.0 times greater than the flutter dynamic pressure for the 20° swept wing.

4. For the AR-7 wings, the transonic dip in the dynamic pressure required for flutter occurred at progressively higher Mach numbers with increasing sweepback angle up to 65°; the transonic dip for the 80° swept wing occurred at a slightly lower Mach number than that for the 65° swept wing.

5. Stiffness requirements established by flutter considerations may be minimized by flight programing of the sweepback angle for wings similar to the present two designs.

Langley Research Center,
National Aeronautics and Space Administration,
Langley Station, Hampton, Va., June 22, 1962.

[redacted]

REFERENCES

1. Staff of the Langley Research Center: The Supersonic Transport - A Technical Summary. NASA TN D-423, 1960.

2. Nichols, Mark R.: The Supersonic Transport - Required Characteristics of Configurations. [Preprint] 341F, Soc. Automotive Eng., 1961.

3. Land, Norman S., Wood, John H., and Foughner, Jerome T., Jr.: An Investigation of the Structural Characteristics of a Simplified Model of a Variable-Sweep Wing. NASA TM X-662, 1962.

4. Stonesifer, John C., and Goetz, Robert C.: Transonic and Supersonic Flutter Trend Investigation of a Variable-Sweep Wing. NASA TM X-598, 1961.

[redacted]

TABLE I.- MASS PROPERTIES OF TYPICAL MODEL

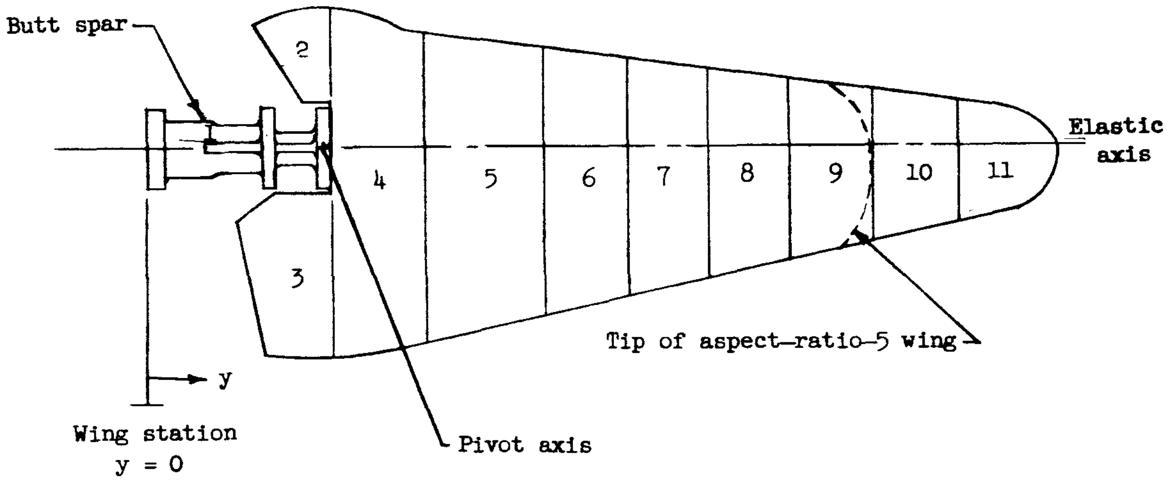

Section number	Section y limits, ft	m_s, slugs/ft	I_α, slug-ft^2/ft	S_α, slug-ft/ft	x_α, ft	y_{cg}, ft
1	0 to 0.187	1.496 × 10^{-2}	9.19 × 10^{-6}	0	0	0.096
2	0.112 to .187	.211	19.33	-218.0 × 10^{-6}	-.10333	.171
3	.089 to .187	.313	38.27	318.0	.10167	.139
4	.187 to .282	1.593	57.89	132.5	.00832	.226
5	.282 to .405	.994	34.15	33.09	.00333	.351
6	.405 to .492	.557	8.33	34.79	.00625	.454
7	.492 to .577	.663	22.60	0	0	.522
8	.577 to .657	.435	9.00	19.88	.00457	.605
9	.657 to .743	.327	4.00	4.08	.00125	.703
10	.743 to .828	.113	.829	6.56	.00583	.789
11	.828 to .929	.142	1.06	4.74	.00333	.870

	Aspect ratio 7	Aspect ratio 5
Total mass (including butt spar), slugs	0.00791	0.00763
Mass from pivot axis to tip, slugs	0.00473	0.00445

[redacted]

TABLE II.- RESONANT VIBRATION FREQUENCIES OF MODELS

Model (a)	Run	$f_{h,1}$, cps	$f_{h,2}$, cps	$f_{h,3}$, cps	f_{yaw}, cps	f_{α}, cps	$g_{h,1}$
Aspect-ratio-7 wings							
I-1	2	74	180	440	230	520	-----
I-1	3	76	196	435	---	510	-----
I-1	4	74	180	440	230	520	0.006
I-1	5, 6, 7	76	196	435	---	510	.008
I-3	8	72	185	442	234	513	.006
I-4	9	74	185	430	233	513	.011
II-1	10	61	153	362	193	420	.007
II-1	11, 13, 15, 18, 20	61	150	344	---	413	.015
II-2	1	60	150	350	---	420	.006
II-2	14, 16, 17	58	151	344	---	417	.012
II-3	12	60	157	360	---	419	.014
II-3	19, 21	61	159	366	---	419	.024
III-1	30	48	125	289	---	343	.006
III-2	24	50	127	300	---	345	.008
III-3	25	47	113	268	155	330	.022
III-4	27	50	126	300	---	340	.007
III-5	29, 34, 37	48	124	290	180	342	.009
III-6	26	48	117	269	---	347	.005
III-6	31, 32	48	126	294	---	343	.008
III-6	33	48	117	265	---	344	.018
III-6	35	48	126	294	---	343	.006
III-7	28	49	121	285	---	352	.005
III-8	36	49	128	291	---	344	.018
III-9	22	48	123	293	---	339	.006
III-10	23	49	125	297	---	338	.007
IV-4	Not tested	38	84	214	130	263	.008
Aspect-ratio-5 wings							
III-3	38	61	196	460	---	348	0.004
III-3	39	61	203	485	---	360	.003
III-3	40	61	196	460	---	348	.003
III-3	41, 42	61	203	485	---	360	.003
IV-1	43	50	175	427	---	297	.011
IV-3	44, 46	46	155	370	156	278	.007
IV-3	51	46	168	399	---	286	.005
IV-3	52, 54, 55	47	176	435	---	293	.006
IV-4	48, 49, 50	47	177	430	---	286	.004
IV-4	53	50	173	431	---	298	.006
IV-4	56, 57, 58	50	170	412	---	299	.006
IV-6	45, 47	46	170	440	---	280	.012

[a]Roman numeral in model designation indicates stiffness level.

TABLE III.- COMPILATION OF RESULTS

(a) Aspect-ratio-7 wing

Model (a)	Run-point number	Model behavior (b)	M	q, lb/sq ft	V, ft/sec	a, ft/sec	T, °R	ρ, slugs/cu ft	μ	$\frac{V}{b\omega_\alpha\sqrt{\mu}}$	q_{adj}, lb/sq ft	f, cps	f/f_α
Λ = 20°													
II-2	1-1	F	0.773	1,205	807	1,045	454	0.00370	38.59	0.391	1,805	185	0.440
I-1	2-1	D	.860	1,787	877	1,020	433	.00464	30.78	.384	1,746	220	.423
I-1	2-2	F	.880	1,928	890	1,012	426	.00486	29.38	.400	1,884	240	.462
I-1	3-1	NF	.872	1,603	900	1,032	444	.00395	36.15	.372	1,628	---	-----
I-1	4-1	F	.907	1,436	917	1,011	426	.00341	41.88	.345	1,403	200	.385
I-1	5-1	NF	.994	2,563	969	975	395	.00545	26.20	.470	2,603	---	-----
I-1	c5-2	F	.914	2,039	891	975	395	.00513	27.84	.419	2,071	240	.470
I-1	6-1	NF	1.041	1,876	1,052	1,011	425	.00339	42.12	.402	1,906	---	-----
I-1	d6-2	F	.948	1,757	965	1,018	431	.00377	37.87	.389	1,785	235	.461
I-1	d6-3	EF	.898	1,670	916	1,020	433	.00398	35.88	.379	1,696	200	.392
I-1	d6-4	NF	.759	1,375	778	1,025	438	.00453	31.52	.344	1,397	---	-----
I-1	7-1	NF	1.078	1,764	1,075	997	414	.00305	46.82	.390	1,792	---	-----
I-1	d7-2	NF	.927	1,565	932	1,006	421	.00360	39.67	.367	1,590	---	-----
I-1	d7-3	NF	.723	1,145	727	1,006	421	.00432	33.06	.314	1,163	---	-----
I-3	8-1	NF	1.128	2,252	1,110	984	403	.00365	39.12	.438	2,261	---	-----
I-3	d8-2	F	.912	1,927	918	1,007	422	.00457	31.25	.405	1,934	230	.448
I-4	9-1	NF	1.124	2,248	1,104	982	401	.00369	38.70	.438	2,257	---	-----
I-4	d9-2	F	.937	1,930	942	1,005	420	.00435	32.82	.405	1,938	225	.438
Λ = 45°													
II-1	10-1	F	0.802	1,594	827	1,032	443	0.00465	30.71	0.450	2,387	250	0.595
II-1	11-1	D	.851	1,305	872	1,024	437	.00343	41.63	.414	2,021	250	.605
II-1	11-2	F	.887	1,452	899	1,013	427	.00359	39.78	.436	2,249	250	.605
II-3	12-1	D	.901	1,382	917	1,018	431	.00328	43.54	.419	2,080	240	.573
II-3	12-2	F	.910	1,423	924	1,016	430	.00333	42.88	.426	2,141	250	.597
II-1	13-1	D	.875	1,207	900	1,028	440	.00298	47.92	.398	1,870	250	.605
II-1	13-2	F	.916	1,338	934	1,020	433	.00306	46.67	.419	2,072	250	.605
II-2	14-1	D	.924	1,355	953	1,032	443	.00298	47.92	.418	2,059	240	.576
II-2	14-2	F	.938	1,413	966	1,030	441	.00302	47.28	.426	2,147	240	.576
II-1	15-1	D	.898	1,204	924	1,029	441	.00281	50.82	.397	1,865	250	.605
II-1	15-2	F	.942	1,318	960	1,019	432	.00286	49.93	.416	2,041	250	.605
II-1	15-3	EF	.962	1,382	976	1,015	429	.00290	49.24	.426	2,140	250	.605
II-2	16-1	BD	.958	1,374	980	1,024	436	.00285	50.10	.420	2,088	250	.600
II-2	16-2	NF	1.108	2,454	1,034	933	363	.00458	31.18	.562	3,728	---	-----
II-2	17-1	NF	1.112	1,973	1,111	999	415	.00319	44.76	.504	2,998	---	-----
II-2	d17-2	F	.975	1,807	977	1,002	418	.00378	37.78	.482	2,746	250	.600
II-1	18-1	BD	.954	1,277	981	1,029	440	.00265	53.89	.409	1,978	250	.605
II-1	d18-2	NF	1.161	2,014	1,140	982	401	.00309	46.21	.514	3,120	---	-----
II-1	d18-3	NF	1.066	1,870	1,054	989	407	.00336	42.50	.495	2,896	---	-----
II-3	19-1	NF	1.157	2,333	1,112	961	384	.00377	37.88	.546	3,511	---	-----
II-3	d19-2	F	1.018	2,133	1,004	986	405	.00423	33.76	.522	3,210	250	.597
II-1	20-1	NF	1.157	2,333	1,112	961	384	.00377	37.88	.554	3,614	---	-----
II-1	d20-2	D	1.018	2,133	1,004	986	405	.00423	33.76	.529	3,304	250	.605
II-1	d20-3	F	.978	2,064	970	992	410	.00438	32.60	.520	3,197	250	.605
II-3	21-1	NF	1.157	2,333	1,112	961	384	.00377	37.88	.546	3,511	---	-----

[a]Roman numeral in model designation indicates stiffness level.

[b]BD denotes short burst of low damping; D denotes start of sustained low damping; NF denotes no flutter; F denotes start of flutter; and EF denotes end of flutter.

[c]Data point obtained during shutdown period (a short period following activation of the close-valve switch during which the tunnel valves are automatically closing).

[d]Data point obtained during period in which tunnel orifice was varied.

[redacted]

[redacted]

TABLE III.- COMPILATION OF RESULTS - Continued

(a) Aspect-ratio-7 wing - Concluded

Model (a)	Run-point number	Model behavior (b)	M	q, lb/sq ft	V, ft/sec	a, ft/sec	T, °R	ρ, slugs/cu ft	μ	$\frac{V}{b\omega_\alpha\sqrt{\mu}}$	q_{adj}, lb/sq ft	f, cps	f/f_α
						Λ = 65°							
III-9	22-1	F	0.789	1,508	816	1,035	445	0.00452	31.59	0.542	3,467	235	0.693
III-10	23-1	F	.914	1,598	934	1,021	434	.00366	39.02	.559	3,695	240	.710
III-2	24-1	F	.973	1,405	986	1,014	428	.00288	49.58	.514	3,119	230	.667
III-3	25-1	BD	.989	1,230	999	1,010	425	.00246	58.05	.503	2,984	216	.654
III-3	25-2	NF	1.107	1,463	1,087	982	401	.00247	57.81	.548	3,549	---	-----
III-6	26-1	F	1.003	1,198	1,017	1,014	428	.00231	61.82	.472	2,628	230	.663
III-4	27-1	F	1.024	1,407	1,052	1,027	439	.00254	56.22	.522	3,216	240	.706
III-7	28-1	NF	1.251	2,992	1,131	904	340	.00467	30.58	.735	6,380	---	-----
III-7	[c]28-2	F	1.199	2,648	1,077	898	336	.00456	31.32	.691	5,646	265	.753
						Λ = 80°							
III-5	29-1	D	0.776	1,473	808	1,041	451	0.00451	31.66	0.531	3,327	235	0.687
III-5	29-2	F	.801	1,594	830	1,037	448	.00461	30.98	.551	3,600	250	.731
III-1	30-1	D	.893	1,607	922	1,033	444	.00377	37.88	.553	3,609	235	.685
III-1	30-2	F	.900	1,814	923	1,026	438	.00425	33.60	.587	4,074	235	.685
III-6	31-1	F	.925	1,464	946	1,022	435	.00327	43.67	.528	3,288	225	.656
III-6	32-1	NF	.938	1,300	962	1,026	438	.00281	50.82	.498	2,919	---	-----
III-6	33-1	D	1.080	1,917	1,080	1,000	416	.00328	43.54	.602	4,280	250	.727
III-6	33-2	F	1.099	2,170	1,086	988	406	.00367	38.91	.640	4,845	250	.727
III-5	34-1	F	1.102	2,590	1,080	980	400	.00444	32.16	.704	5,850	266	.778
III-6	35-1	F	1.114	2,323	1,091	979	399	.00390	36.62	.665	5,216	255	.743
III-8	36-1	D	1.154	2,170	1,139	987	406	.00334	42.75	.641	4,845	245	.712
III-8	[c]36-2	F	1.043	1,832	1,038	995	412	.00339	42.12	.588	4,090	250	.727
III-5	37-1	F	1.200	2,765	1,159	966	388	.00411	34.74	.728	6,245	248	.725

[a]Roman numeral in model designation indicates stiffness level.

[b]BD denotes short burst of low damping; D denotes start of sustained low damping; NF denotes no flutter; F denotes start of flutter; and EF denotes end of flutter.

[c]Data point obtained during shutdown period (a short period following activation of the close-valve switch during which the tunnel valves are automatically closing).

[redacted]

TABLE III.- COMPILATION OF RESULTS - Concluded

(b) Aspect-ratio-5 wing

Model (a)	Run-point number	Model behavior (b)	M	q, lb/sq ft	V, ft/sec	a, ft/sec	T, °R	ρ, slugs/cu ft	μ	$\frac{V}{b\omega_\alpha\sqrt{\mu}}$	q_{adj}, lb/sq ft	f, cps	f/f_α
$\Lambda = 20^\circ$													
III-3	38-1	D	0.768	1,332	795	1,035	446	0.00421	34.20	0.458	919	160	0.460
III-3	38-2	F	.780	1,479	804	1,031	443	.00456	31.58	.484	1,020	157	.451
III-3	39-1	D	.849	1,446	878	1,034	445	.00375	38.40	.461	932	128	.356
III-3	39-2	F	.869	1,639	893	1,028	440	.00410	35.12	.492	1,056	128	.356
III-3	40-1	F	.907	1,289	934	1,019	432	.00301	47.84	.455	889	125	.359
III-3	40-2	EF	.956	1,431	965	1,010	424	.00307	46.90	.475	987	125	.359
III-3	40-3	NF	1.019	1,869	1,002	983	402	.00372	38.71	.543	1,289	---	-----
III-3	41-1	F	.931	1,328	958	1,029	440	.00289	49.83	.442	856	122	.339
III-3	42-1	NF	1.146	2,899	1,091	952	377	.00487	29.57	.653	1,868	---	-----
IV-1	43-1	F	.864	1,076	896	1,038	448	.00267	53.93	.482	1,019	108	.364
$\Lambda = 45^\circ$													
IV-3	44-1	F	0.785	1,319	814	1,037	447	0.00398	36.18	0.571	1,425	140	0.504
IV-6	45-1	D	.796	1,094	828	1,041	451	.00318	45.28	.516	1,165	137	.489
IV-6	45-2	F	.822	1,210	852	1,036	447	.00333	43.24	.542	1,289	137	.489
IV-3	46-1	F	.877	1,230	900	1,026	438	.00303	47.52	.551	1,329	129	.464
IV-6	47-1	NF	.897	1,138	917	1,023	435	.00270	53.33	.527	1,212	---	-----
IV-4	48-1	D	1.051	1,365	1,059	1,008	423	.00243	59.26	.564	1,394	113	.395
IV-4	48-2	F	1.146	1,669	1,133	989	407	.00260	55.38	.624	1,704	128	.448
IV-4	49-1	D	1.104	1,516	1,098	995	412	.00251	57.37	.595	1,548	125	.437
IV-4	49-2	F	1.141	1,761	1,123	985	403	.00279	51.61	.641	1,798	130	.454
IV-4	[c]49-3	EF	1.075	1,624	1,063	989	407	.00287	50.17	.616	1,658	125	.437
IV-4	50-1	D	1.226	2,408	1,178	961	384	.00374	38.50	.779	2,459	150	.524
IV-4	50-2	F	1.223	2,694	1,165	953	378	.00397	36.27	.794	2,751	155	.542
$\Lambda = 65^\circ$													
IV-3	51-1	NF	0.786	2,554	752	957	381	0.00902	15.96	0.773	2,608	---	-----
IV-3	52-1	D	.858	2,542	874	1,019	432	.00665	21.65	.752	2,473	157	0.536
IV-3	52-2	F	.838	3,066	806	961	385	.00944	15.25	.827	2,983	159	.543
IV-4	53-1	D	1.015	3,649	951	937	366	.00806	17.87	.885	3,432	166	.556
IV-4	[d]53-2	F	.966	3,282	901	937	366	.00808	17.82	.840	3,087	166	.556
IV-3	54-1	NF	1.113	3,874	1,027	922	354	.00734	19.62	.928	3,769	---	-----
IV-3	55-1	NF	1.215	3,266	1,123	924	356	.00518	27.80	.853	3,177	---	-----
$\Lambda = 80^\circ$													
IV-4	56-1	NF	0.838	2,395	843	1,006	421	0.00673	21.40	0.714	2,237	---	-----
IV-4	57-1	NF	1.096	2,824	1,052	960	384	.00510	28.24	.777	2,638	---	-----
IV-4	58-1	NF	1.209	3,228	1,137	940	368	.00499	28.86	.830	3,016	---	-----

[a]Roman numeral in model designation indicates stiffness level.

[b]BD denotes short burst of low damping; D denotes start of sustained low damping; NF denotes no flutter; F denotes start of flutter; and EF denotes end of flutter.

[c]Data point obtained during period in which tunnel orifice was varied.

[d]Data point obtained during shutdown period (a short period following activation of the close-valve switch during which the tunnel valves are automatically closing).

[redacted]

[redacted]

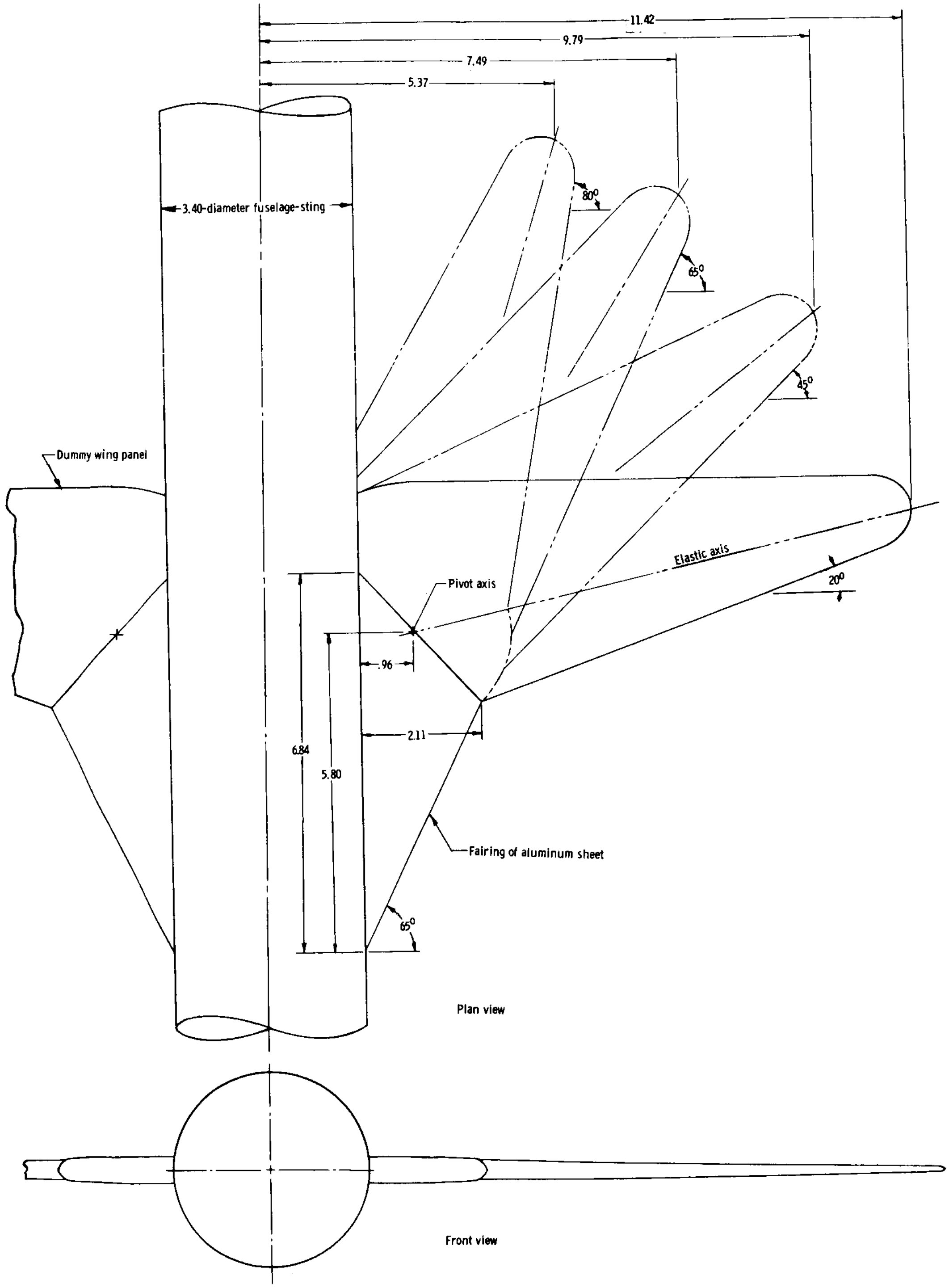

(a) Aspect-ratio-7 wing shown mounted at the sweepback angles investigated.

Figure 1.- Sketches of models. All linear dimensions are in inches.

[redacted]

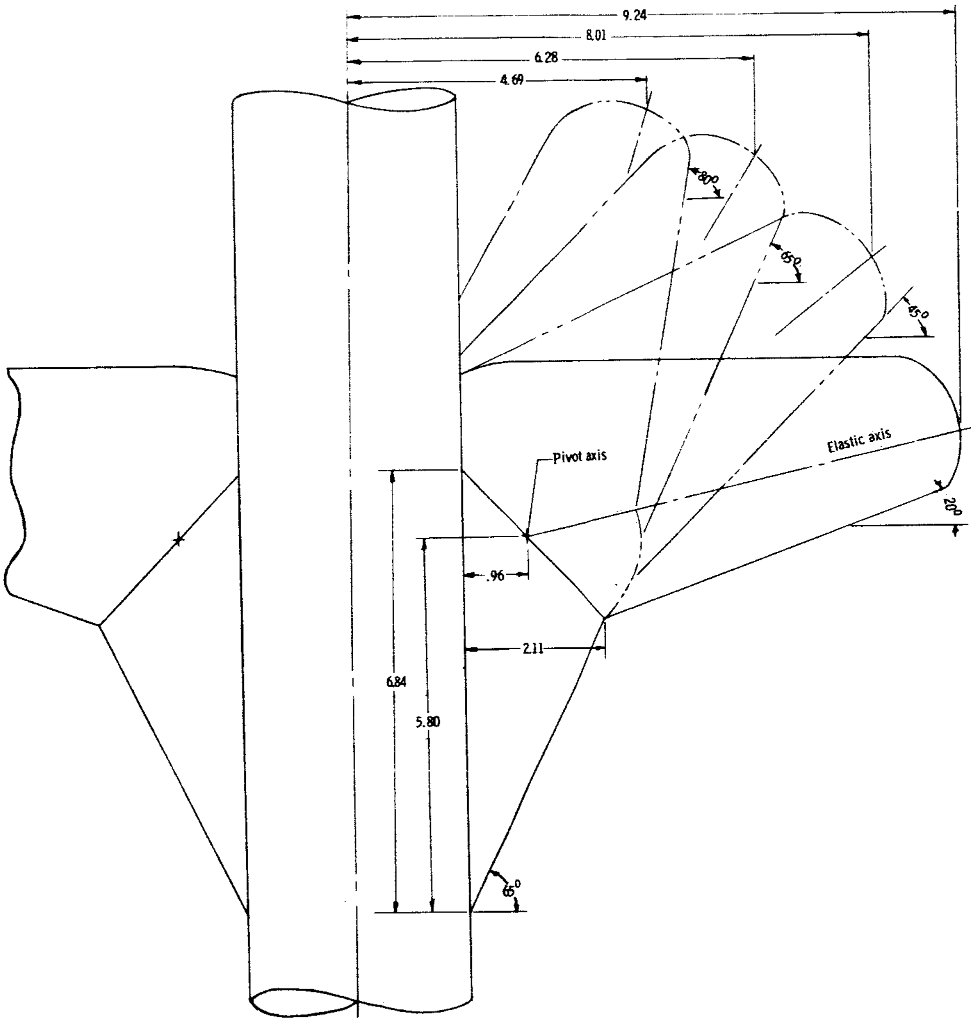

(b) Aspect-ratio-5 wing shown mounted at the sweepback angles investigated.

Figure 1.- Continued.

[redacted]

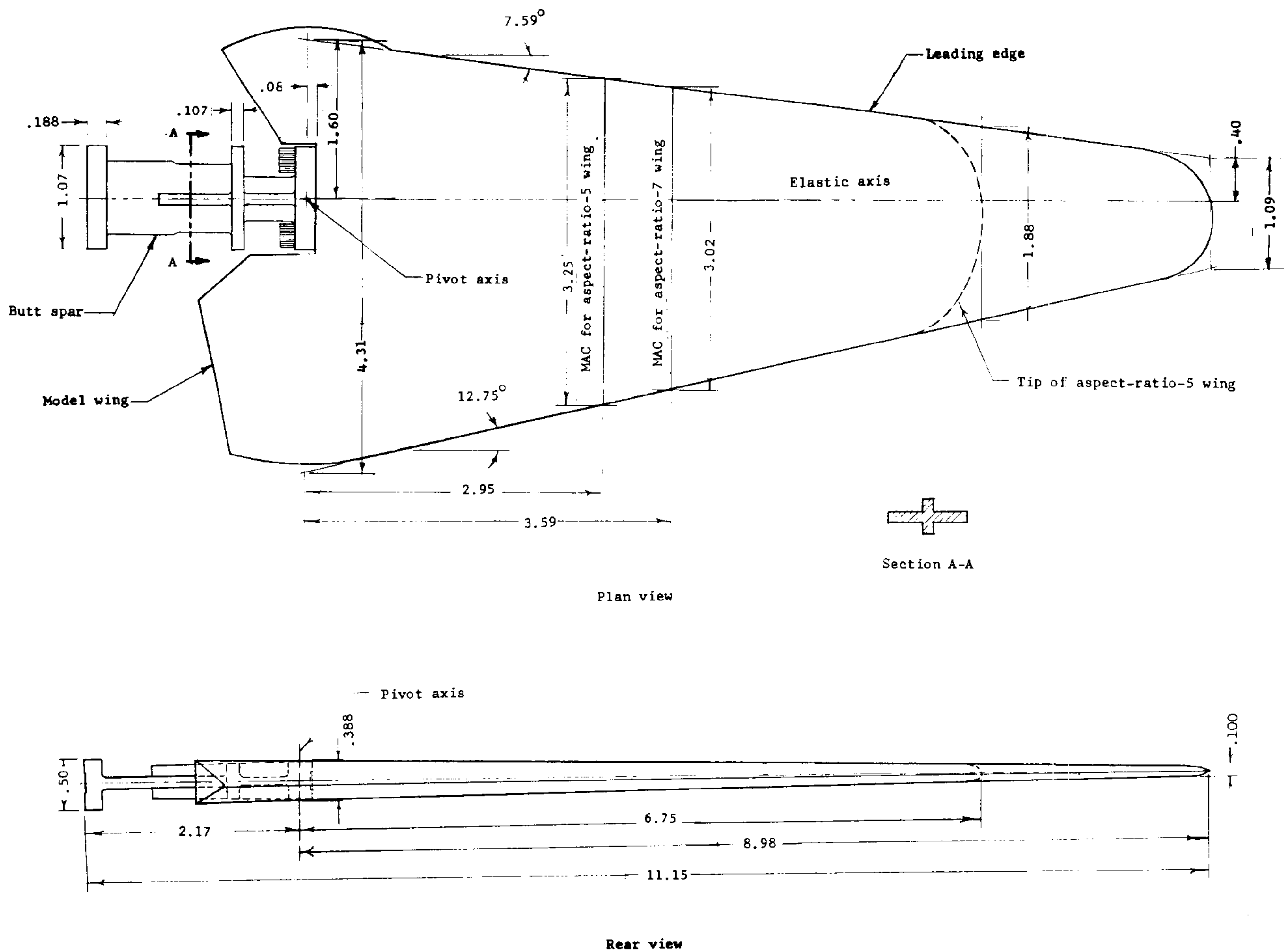

(c) Model wing with butt spar attached.

Figure 1.- Concluded.

[redacted]

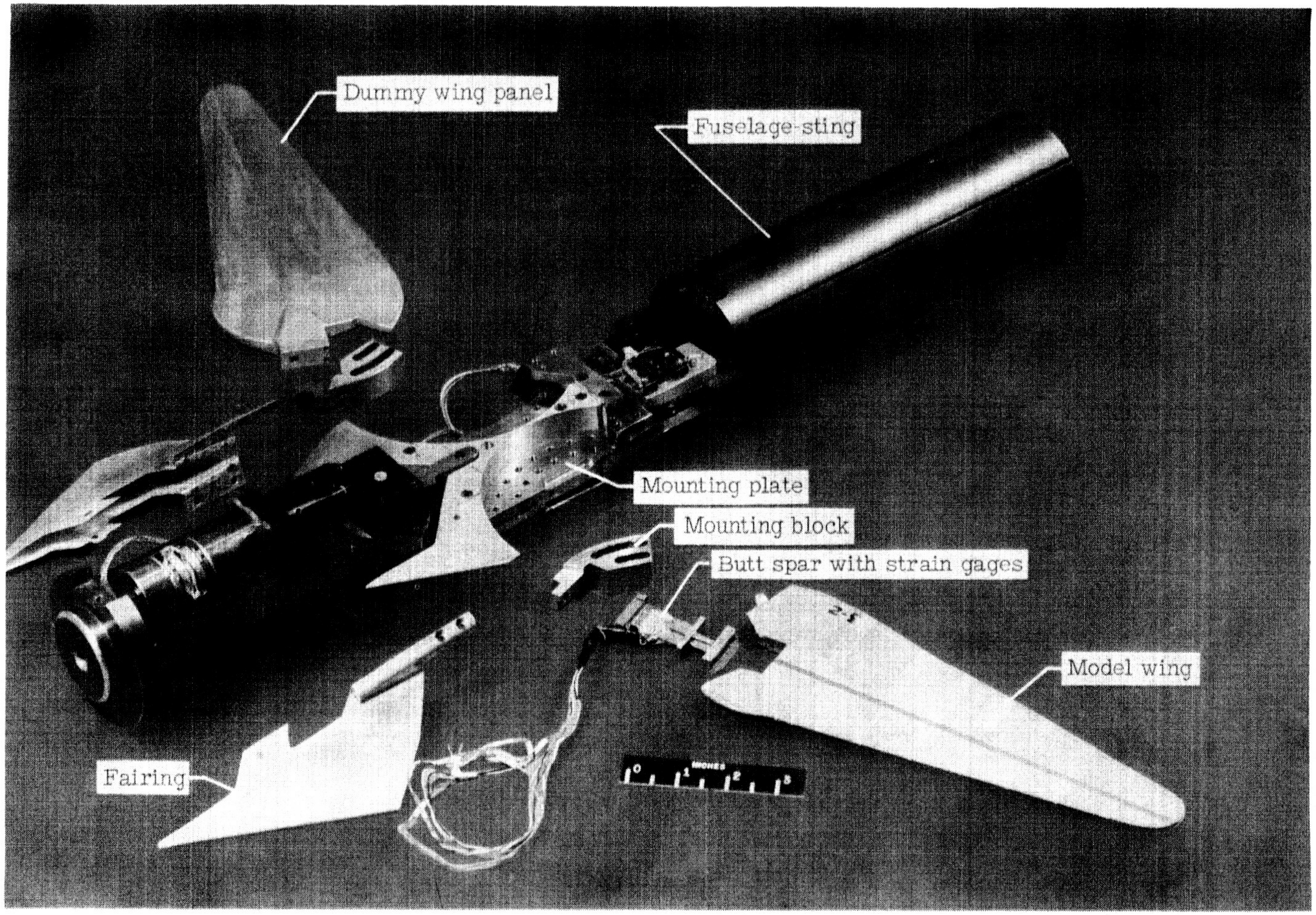

L-61-867.1

(a) Exploded view of mounting system and aspect-ratio-7 wing.

Figure 2.- Photographs of models.

[redacted]

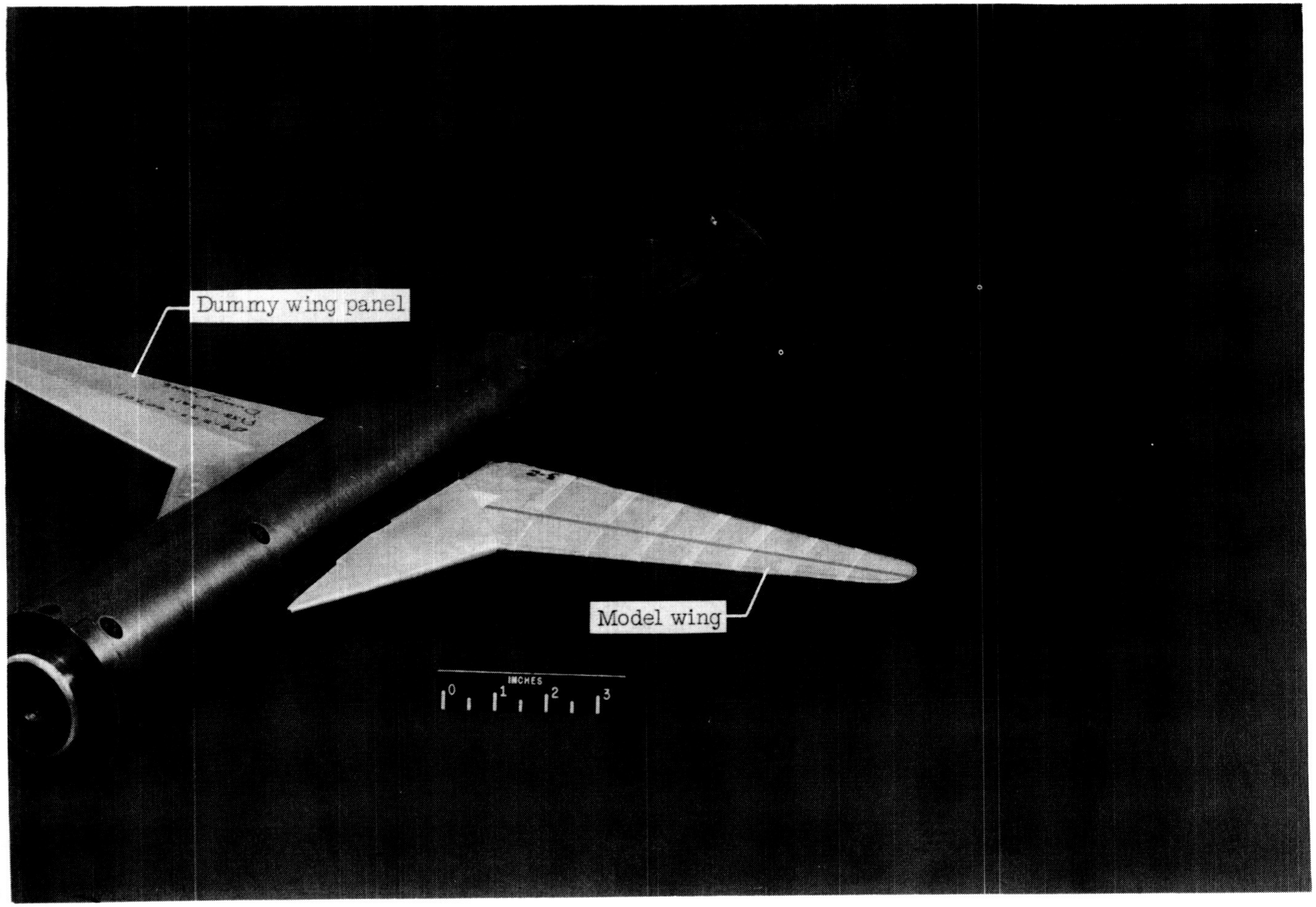

L-61-873.1

(b) View of aspect-ratio-7 wing mounted at 20° sweepback angle.

Figure 2.- Continued.

[redacted]

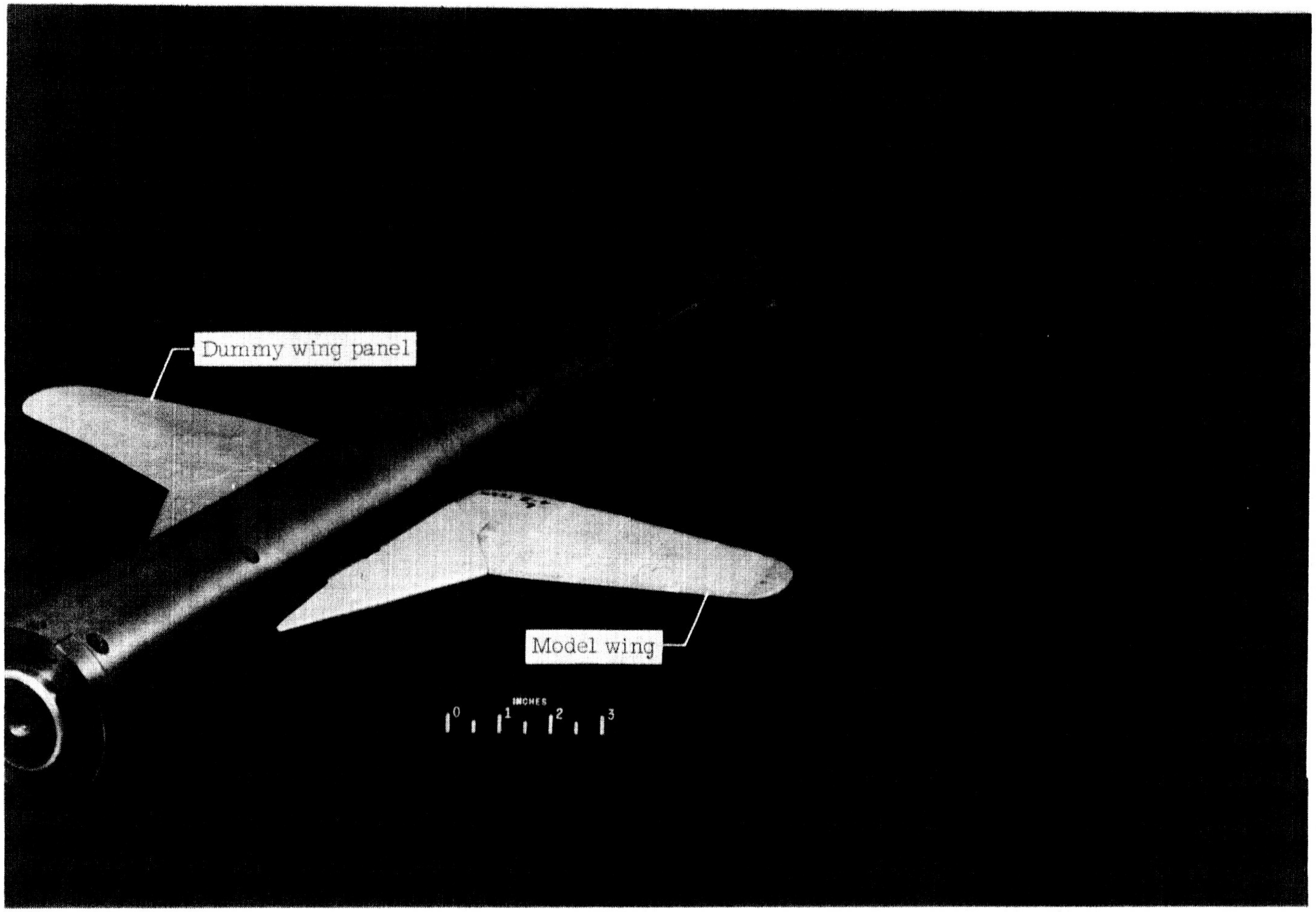

L-61-872.1

(c) View of aspect-ratio-5 wing mounted at 20° sweepback angle.

Figure 2.- Concluded.

[redacted]

[redacted]

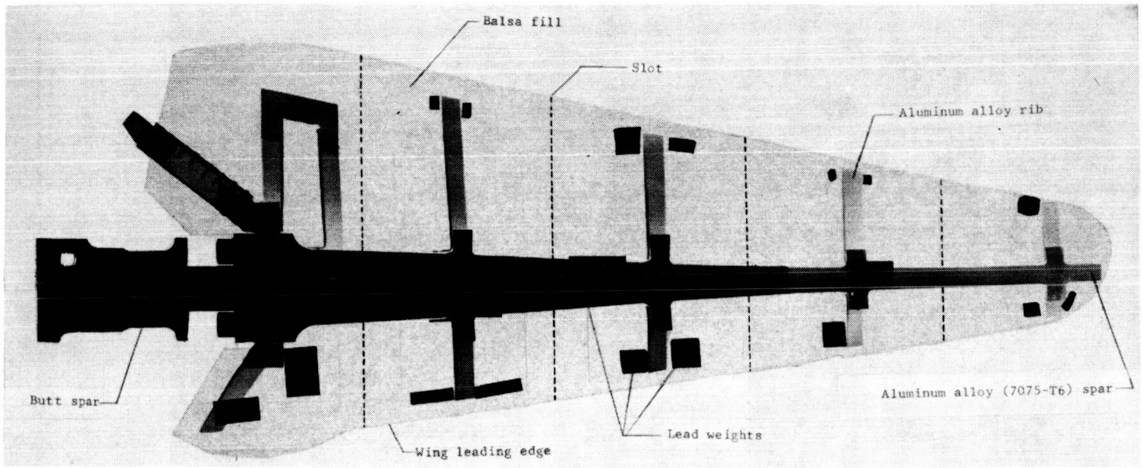

(a) Typical wing of stiffness level I.

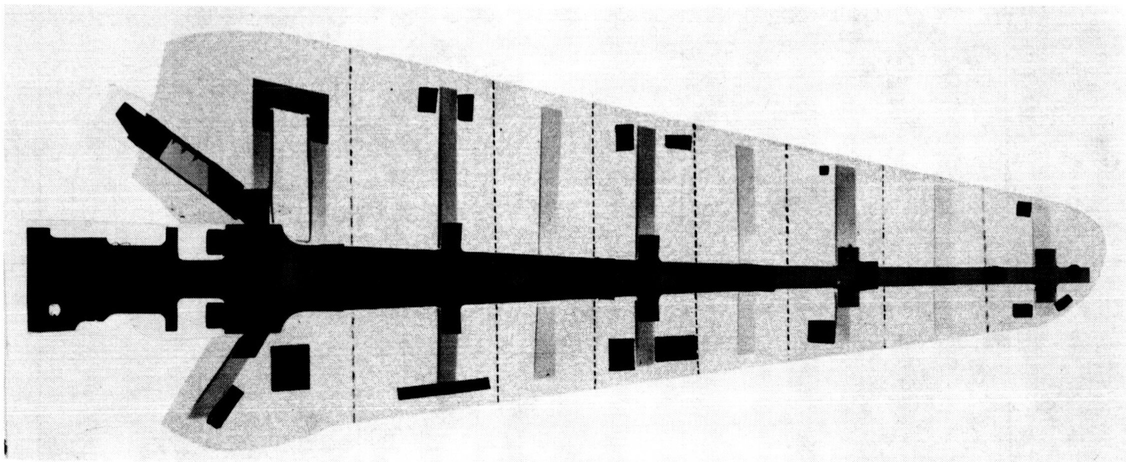

(b) Typical wing of stiffness levels II, III, and IV. L-62-2112

Figure 3.- X-ray photographs of typical wings. Broken lines were added to indicate slot locations.

[redacted]

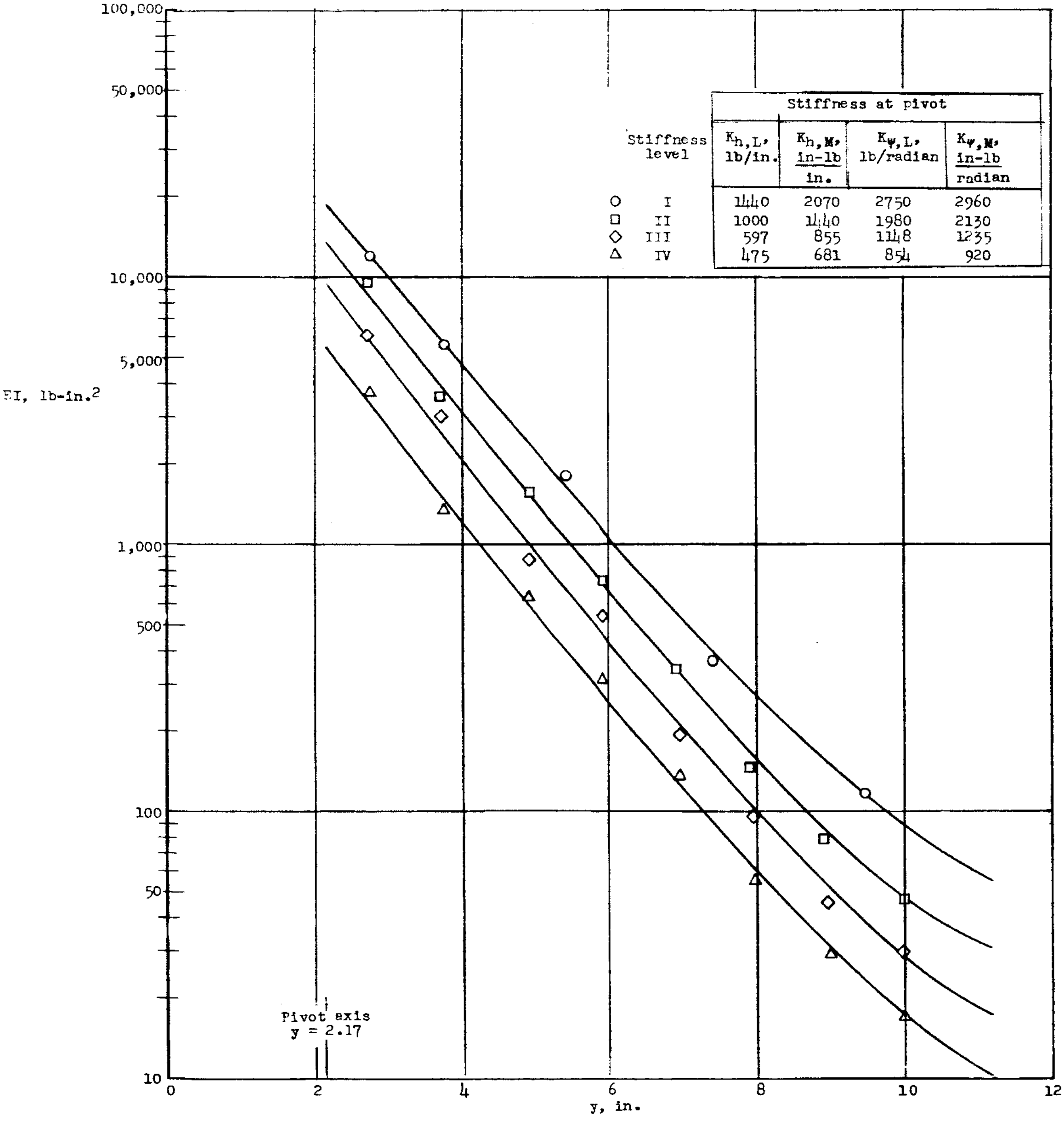

(a) Bending stiffness.

Figure 4.- Measured spanwise distribution of bending and torsional stiffness for a typical wing of each stiffness level.

[redacted]

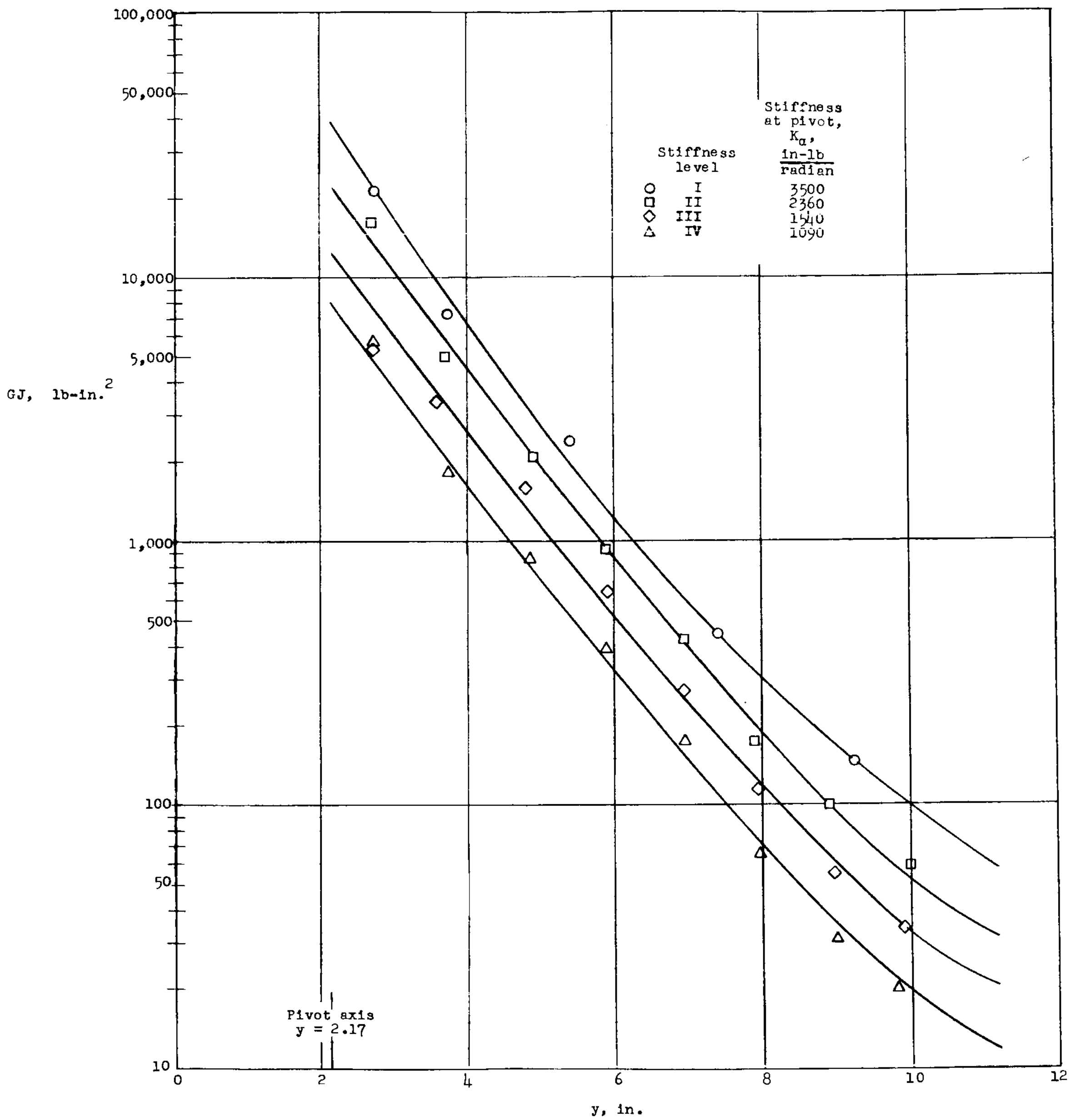

(b) Torsional stiffness.

Figure 4.- Concluded.

[redacted]

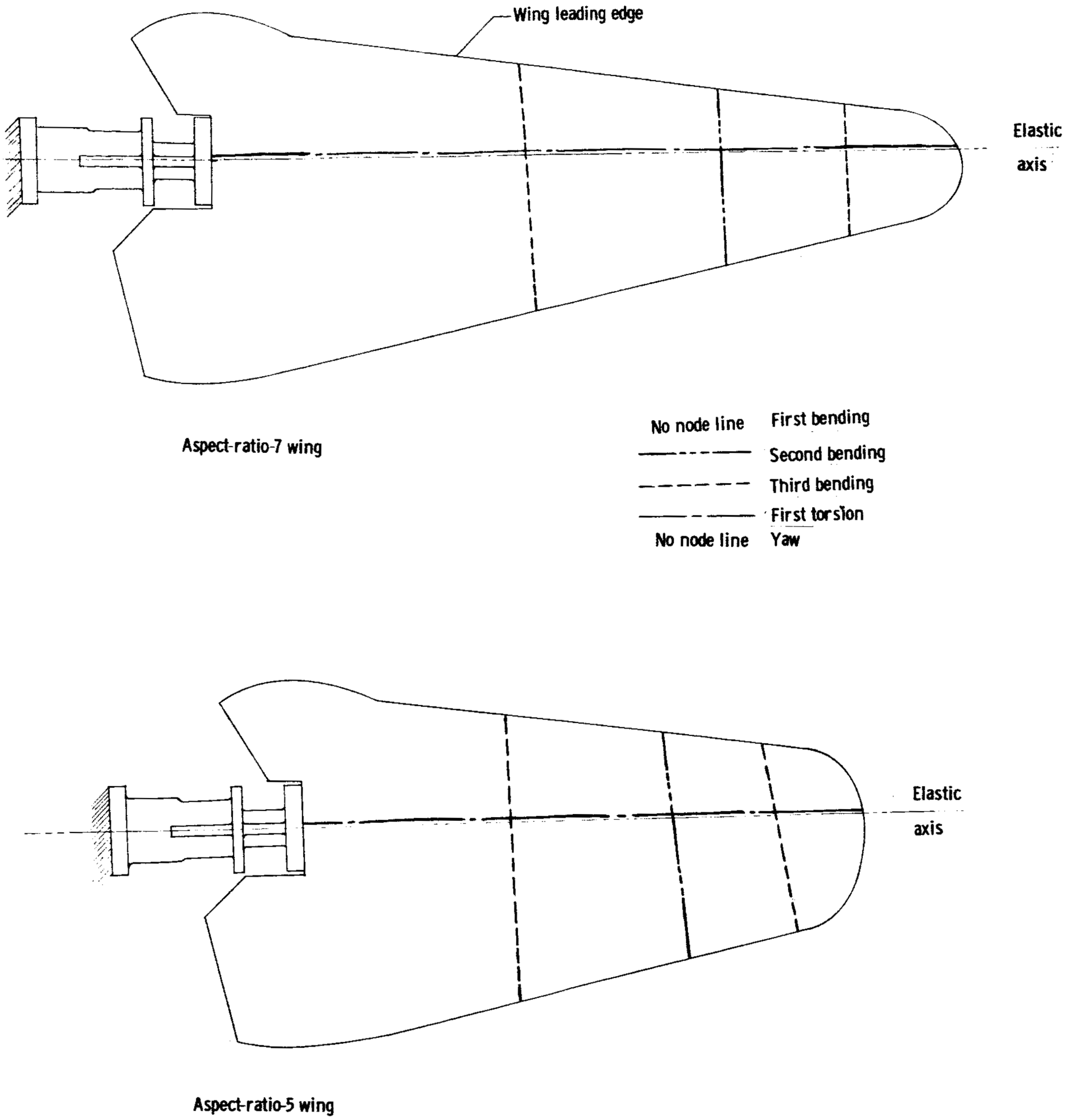

Figure 5.- Typical node lines associated with measured vibration modes of model.

[redacted]

[redacted]

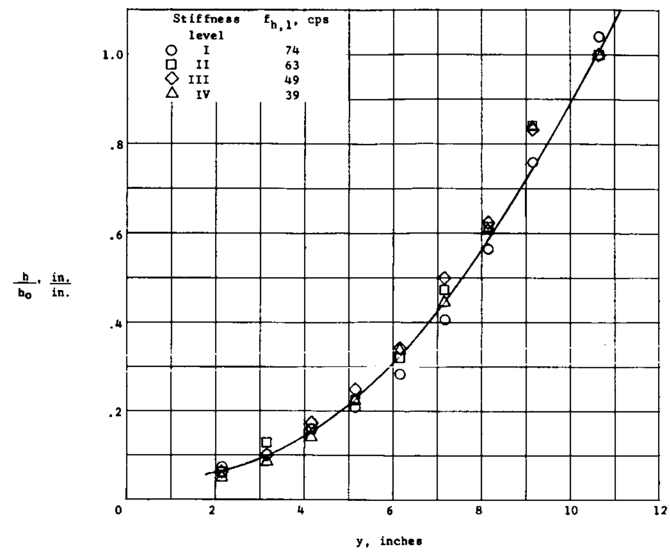

(a) First bending mode.

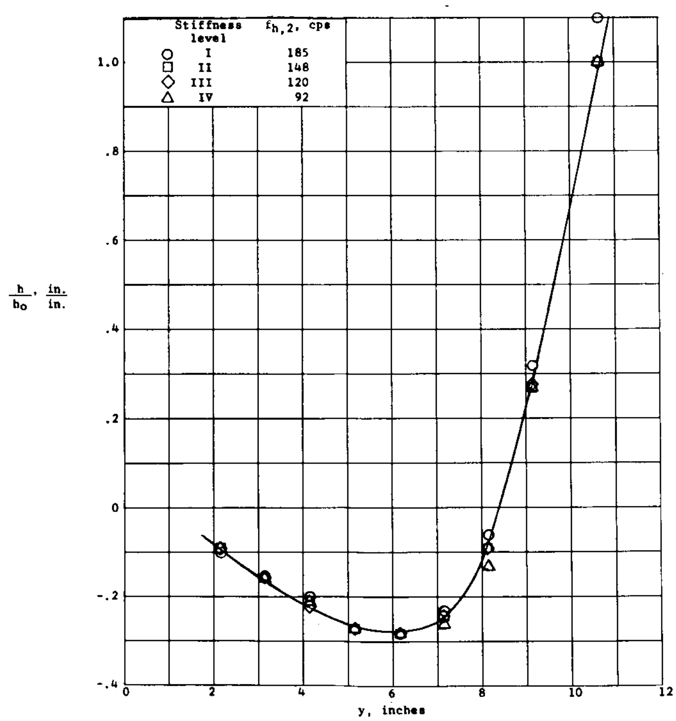

(b) Second bending mode.

Figure 6.- Measured mode shapes of vibration modes of typical aspect-ratio-7 models.

[redacted]

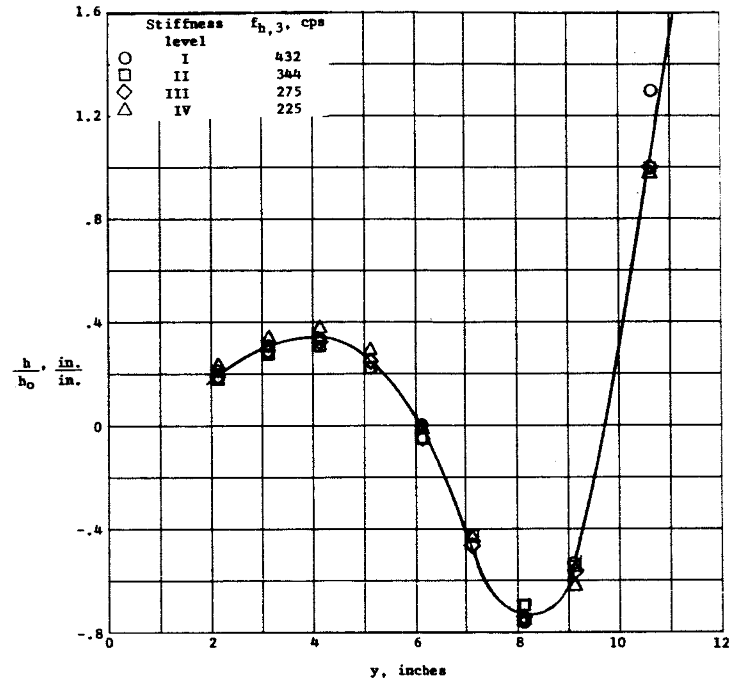

(c) Third bending mode.

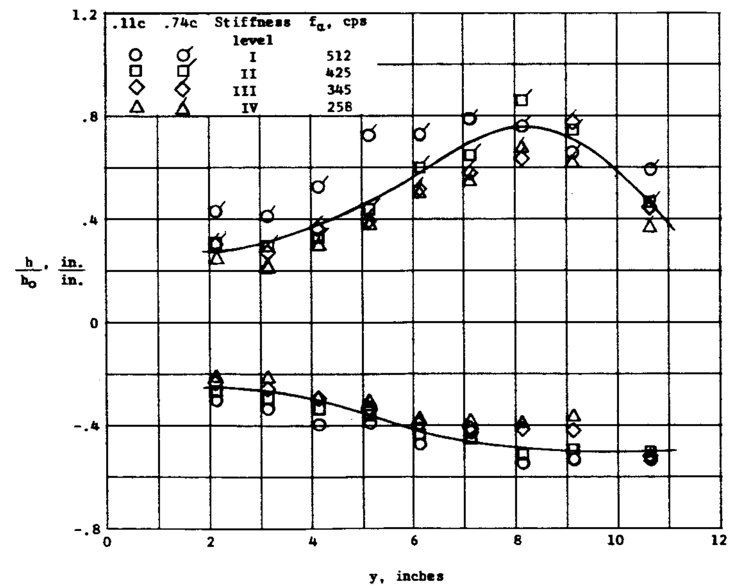

(d) First torsion mode.

Figure 6.- Concluded.

[redacted]

[redacted]

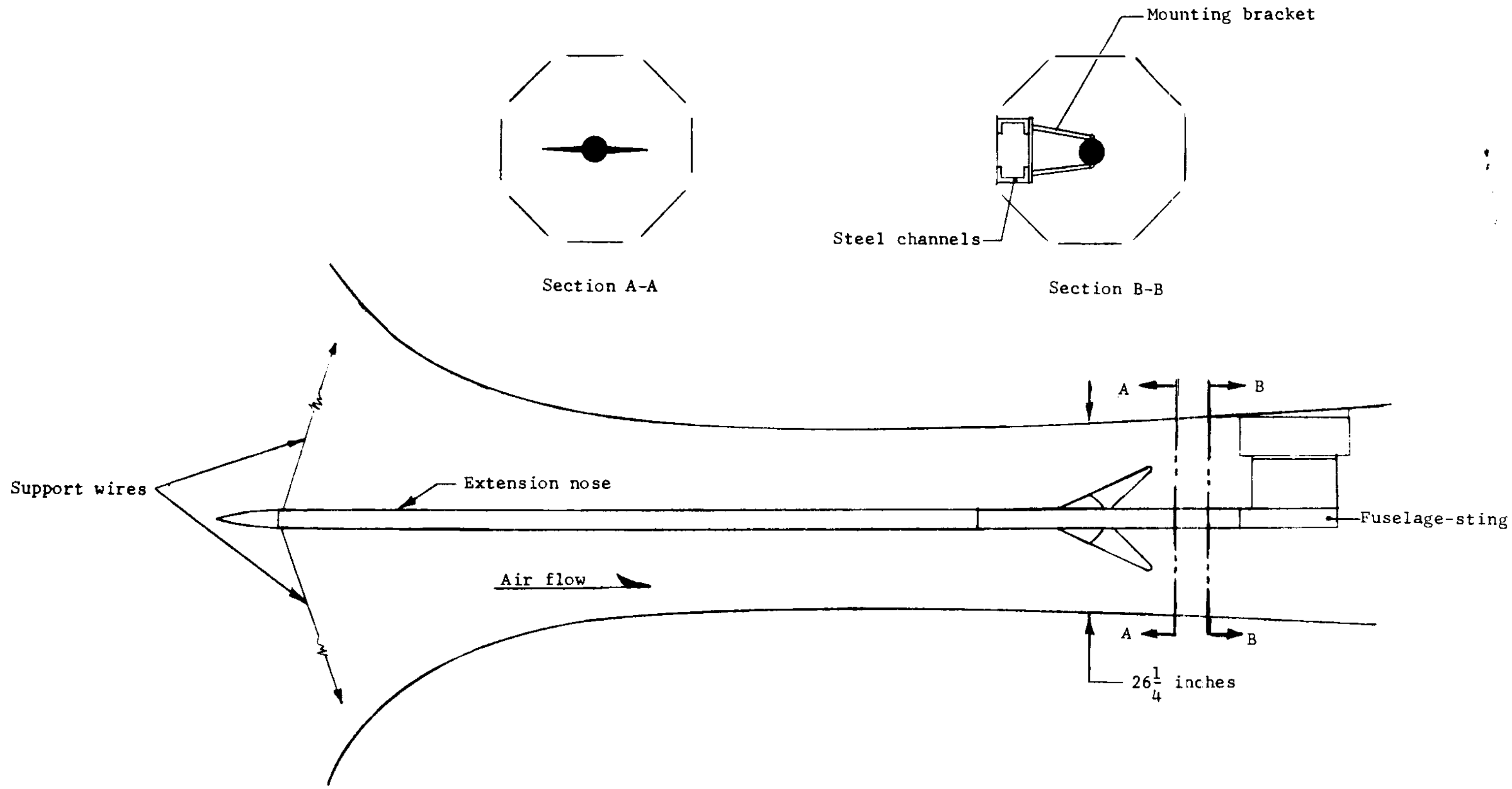

Figure 7.- Sketch of Langley transonic blowdown tunnel showing an aspect-ratio-7 wing installed at 65° sweepback angle with the fuselage-sting at the center-line location.

[redacted]

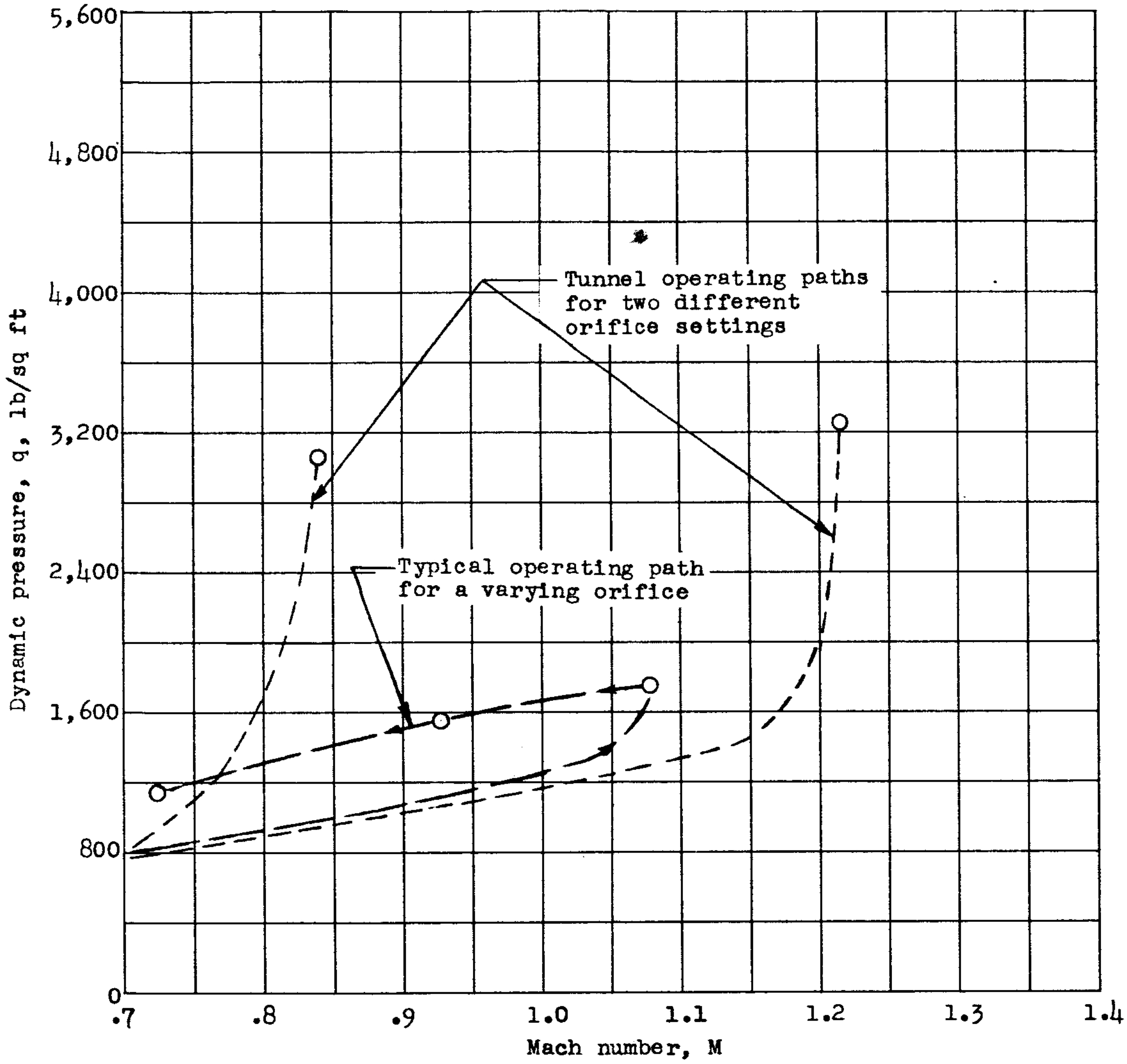

Figure 8.- Variation of dynamic pressure with Mach number during three typical runs in the Langley transonic blowdown tunnel.

[redacted]

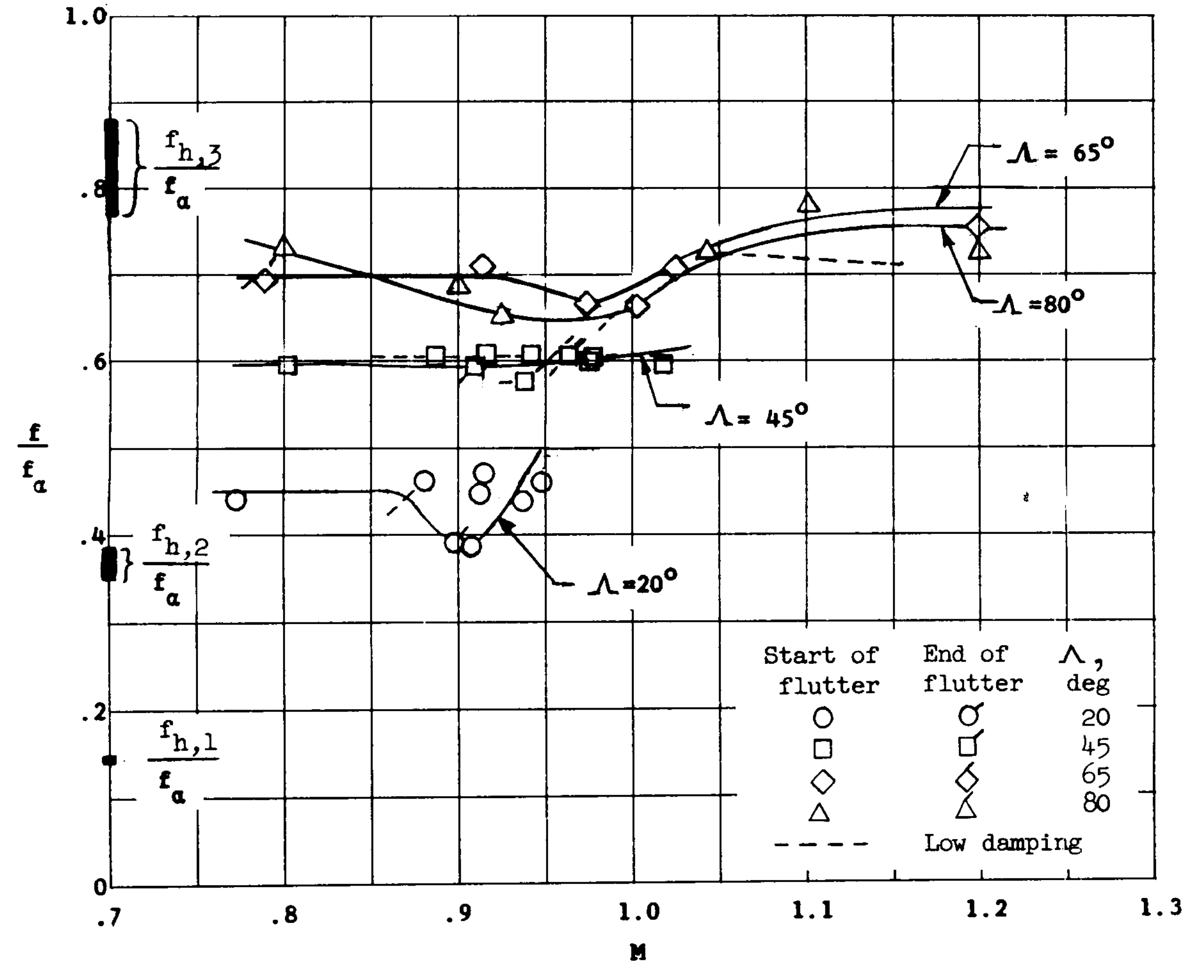

(a) Aspect-ratio-7 wing.

Figure 9.- Variation of ratio of flutter frequency to first-torsion frequency with Mach number for wing planforms investigated.

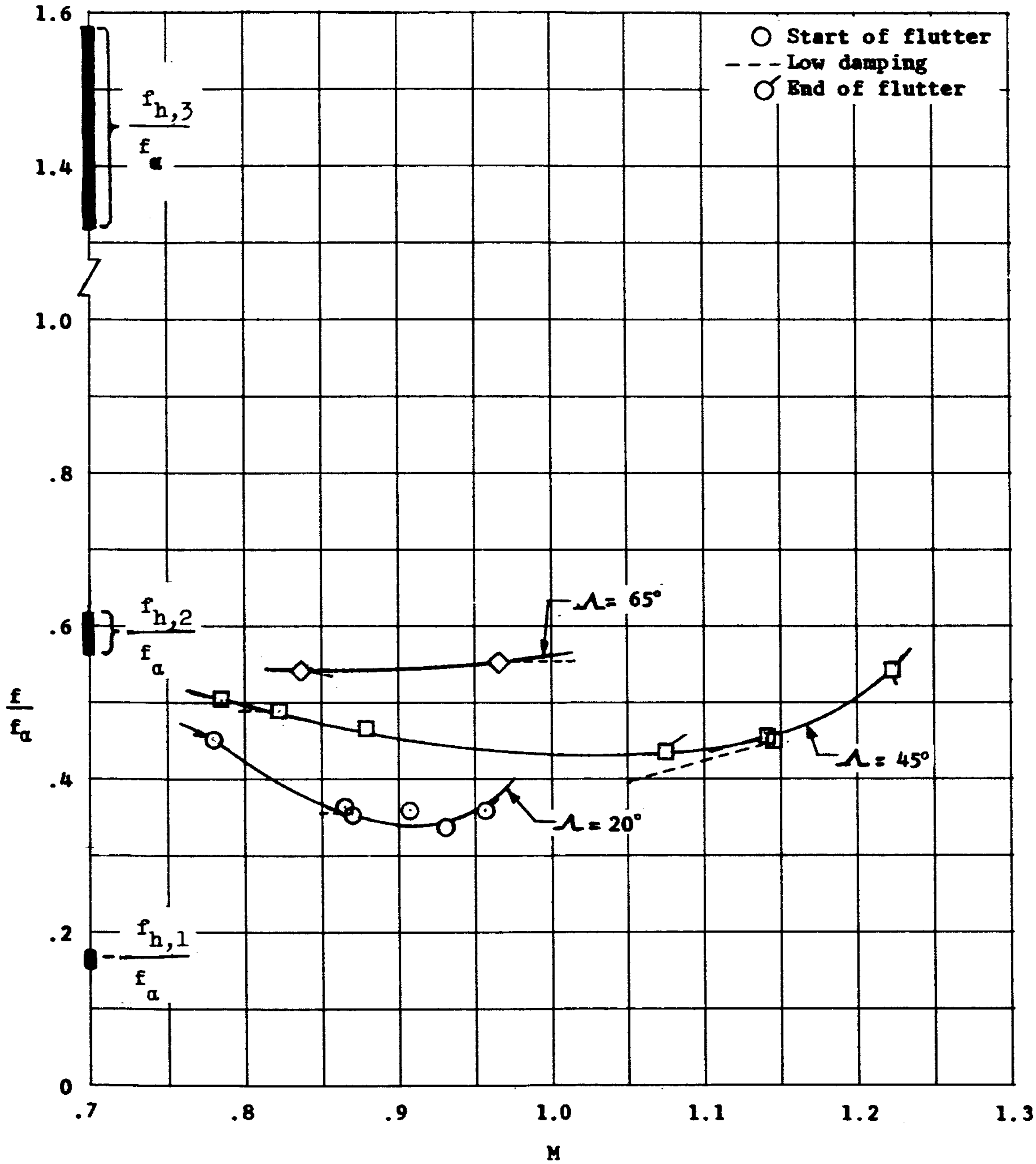

(b) Aspect-ratio-5 wing.

Figure 9.- Concluded.

[redacted]

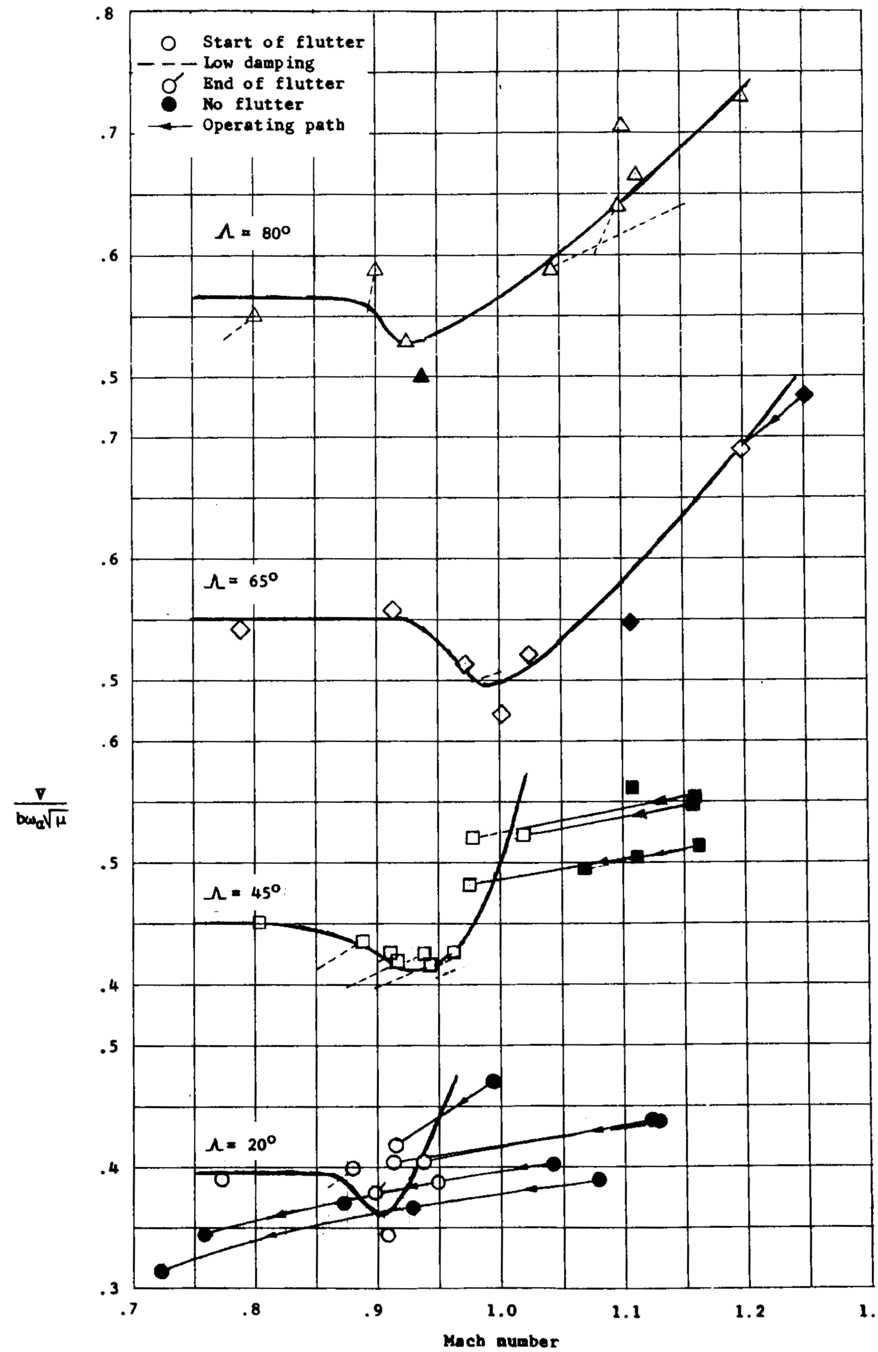

(a) Aspect-ratio-7 wing.

Figure 10.- Variation of flutter-speed index with Mach number for wing planforms investigated.

[redacted]

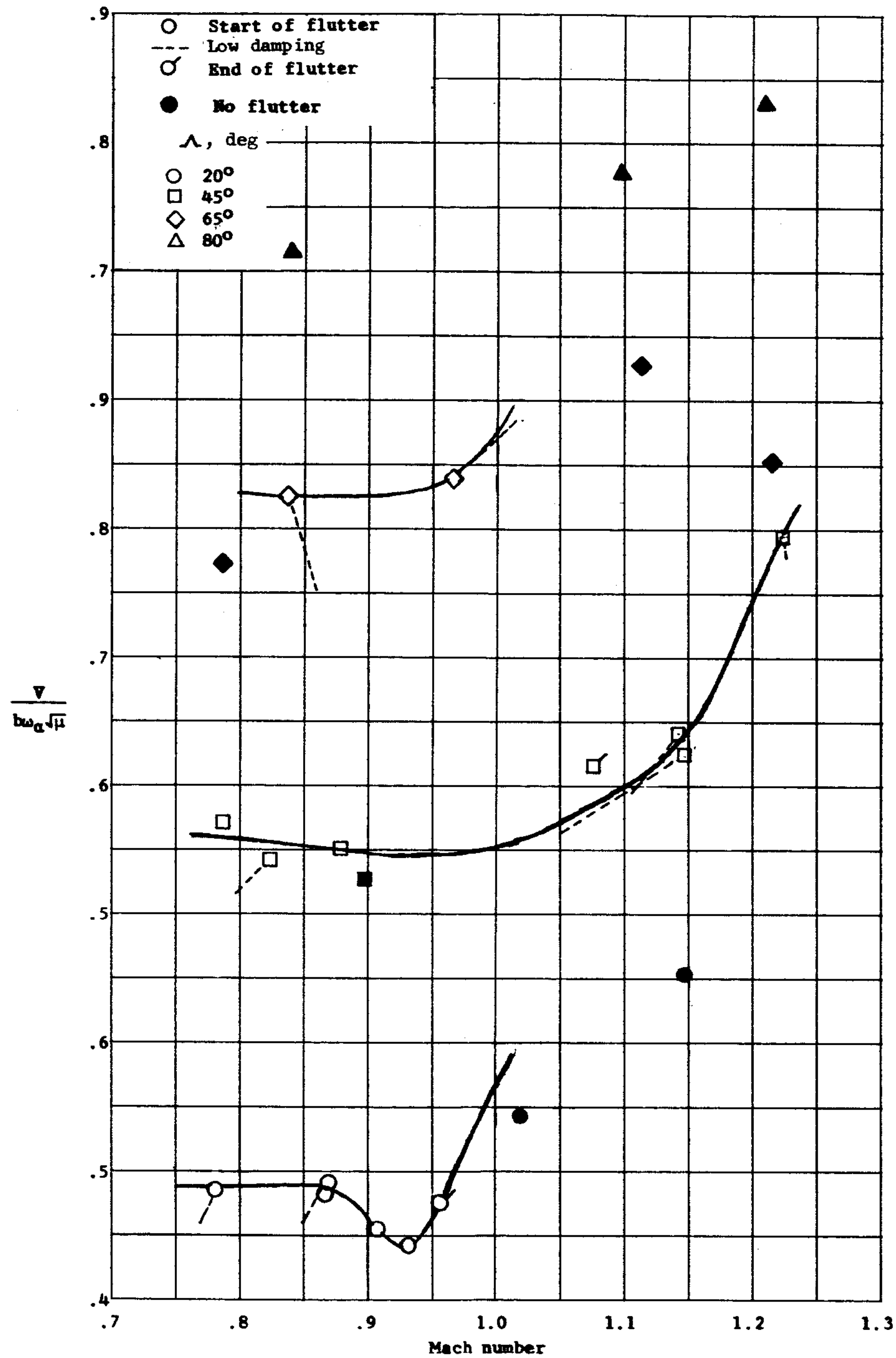

(b) Aspect-ratio-5 wing.

Figure 10.- Concluded.

[redacted]

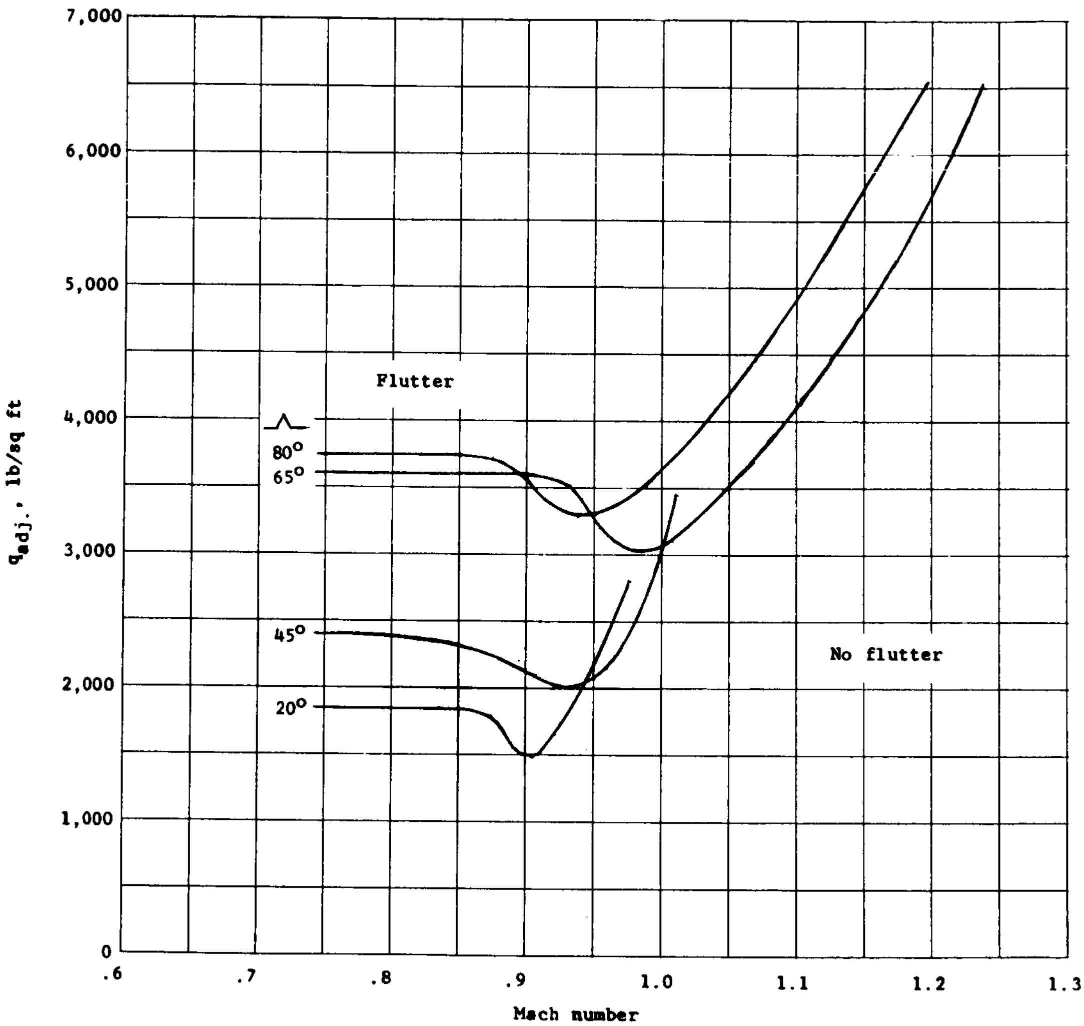

Figure 11.- Variation with Mach number of dynamic pressure applicable to an aspect-ratio-7 wing of stiffness level I at the various sweepback angles.

[redacted]

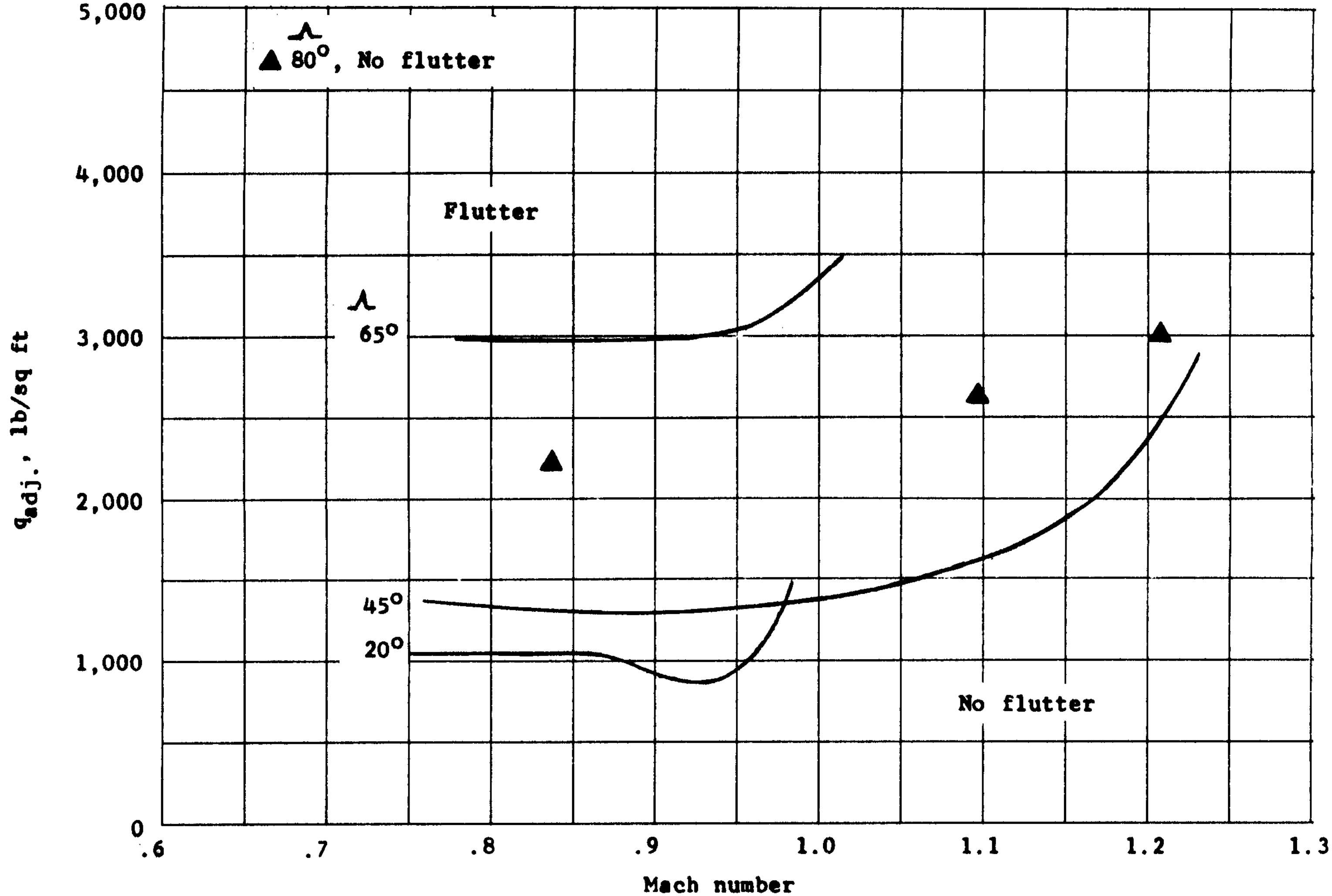

Figure 12.- Variation with Mach number of dynamic pressure applicable to an aspect-ratio-5 wing of stiffness level IV at the various sweepback angles.

[redacted]

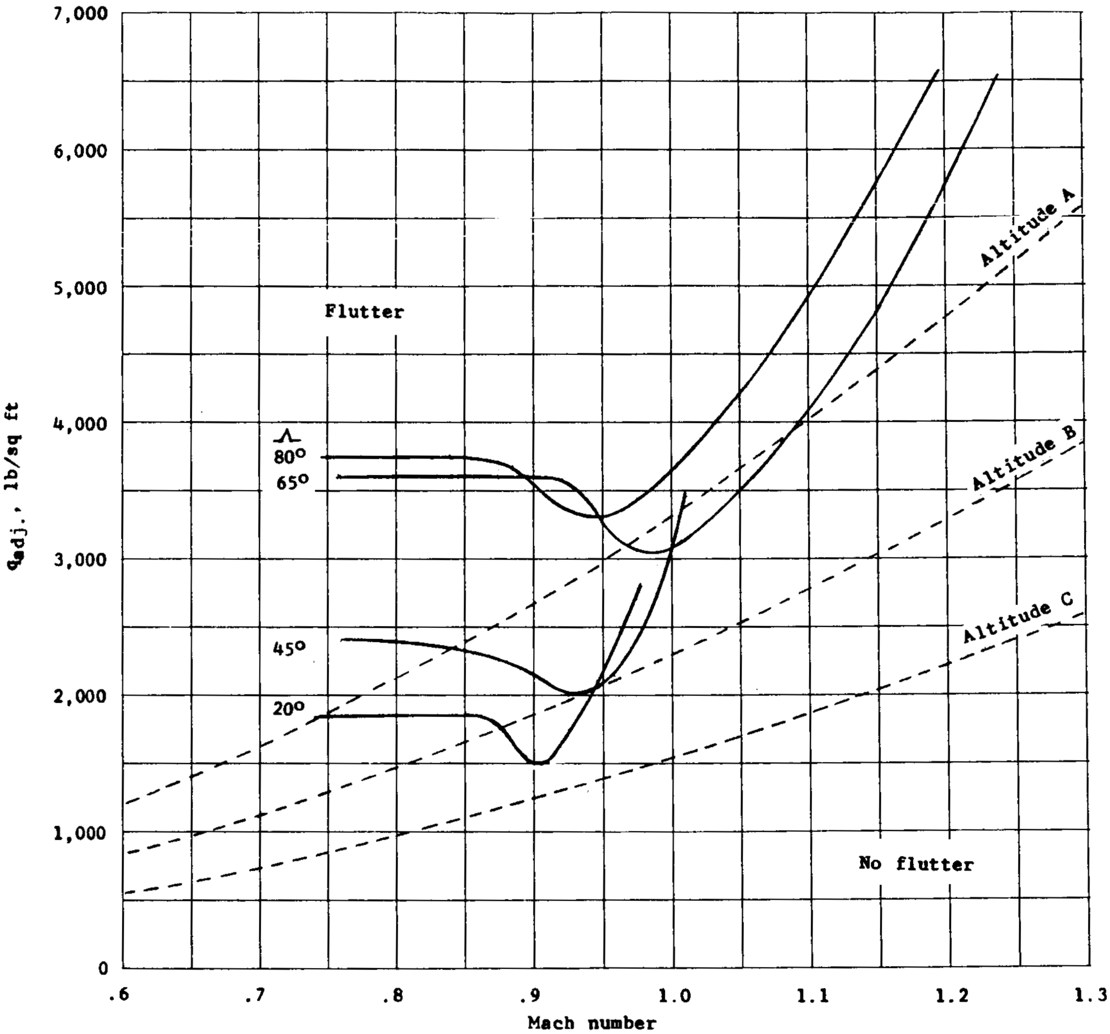

Figure 13.- Flutter boundaries for the aspect-ratio-7 wing and three typical altitude lines. The dynamic pressures for the altitude lines have been increased by 32 percent to provide a flutter safety margin.

[redacted]

L-1719 NASA-Langley, 1962